

ตัวเร่งปฏิกิริยานิกเกิล-รูทีเนียมบนซีเรียมเซอร์โคเนียออกไซด์สำหรับดรายรีฟอร์มมิงของมีเทน



นางสาวญาดา มาคุ้ม

สถาบันวิทยบริการ

จุฬาลงกรณ์มหาวิทยาลัย

วิทยานิพนธ์นี้เป็นส่วนหนึ่งของการศึกษาตามหลักสูตรปริญญาวิทยาศาสตรมหาบัณฑิต

สาขาวิชาปิโตรเคมีและวิทยาศาสตร์พอลิเมอร์

คณะวิทยาศาสตร์ จุฬาลงกรณ์มหาวิทยาลัย

ปีการศึกษา 2549

ลิขสิทธิ์ของจุฬาลงกรณ์มหาวิทยาลัย

Ni-Ru CATALYSTS ON CERIUM ZIRCONYL OXIDE FOR  
DRY REFORMING OF METHANE



Miss Yada Makhum

สถาบันวิทยบริการ  
A Thesis Submitted in Partial Fulfillment of the Requirements  
for the Degree of Master of Science Program in Petrochemistry and Polymer Science

Faculty of Science

Chulalongkorn University

Academic year 2006

Copyright of Chulalongkorn University

Thesis Title Ni-Ru CATALYSTS ON CERIUM ZIRCONYL OXIDE FOR  
DRY REFORMING OF METHANE  
By Miss Yada Makhum  
Field of Study Petrochemistry and Polymer Science  
Thesis Advisor Associate Professor Supawan Tantayanon

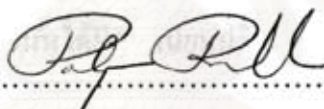
---

Accepted by the Faculty of Science, Chulalongkorn University in Partial  
Fulfillment of the Requirements for the Master's Degree

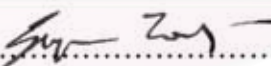


..... Dean of the Faculty of Science  
(Professor Piamsak Menasveta, Ph.D.)

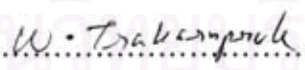
#### THESIS COMMITTEE



..... Chairman  
(Professor Pattarapan Prasassarakich, Ph.D.)



..... Thesis Advisor  
(Associate Professor Supawan Tantayanon, Ph.D.)



..... Member  
(Associate Professor Wimonrat Trakarnpruk, Ph.D.)



..... Member  
(Assistant Professor Warinthorn Chavasiri, Ph.D.)

ฉวาคา มาคุ่ม: ตัวเร่งปฏิกิริยานิกเกิล-รูทีเนียมบนซีเรียมเซอร์โคเนียมออกไซด์สำหรับ  
 ครายรีฟอร์มมิงของมีเทน (Ni-Ru CATALYSTS ON CERIUM ZIRCONYL OXIDE  
 FOR DRY REFORMING OF METHANE) อ.ที่ปรึกษา: รศ. ดร. ศุภวรรณ ตันคยานนท์;  
 68 หน้า.

งานวิจัยนี้ได้ใช้ไมโครอิมัลชันแบบน้ำในน้ำมันในการเตรียม  $Ce_{1-x}Zr_xO_2$  มิกซ์ออกไซด์ซึ่ง  
 ใช้เป็นตัวรองรับ ได้ใช้วิธีการฝังตัวในการฝังนิกเกิล 15 เปอร์เซ็นต์บนตัวรองรับ ได้ปรับอัตราส่วน  
 ของ  $CeO_2$  และ  $ZrO_2$  อย่างเป็นระบบ ได้พิสูจน์เอกลักษณ์ของตัวเร่งปฏิกิริยาที่เตรียมได้ด้วยเทคนิค  
 ทางกายภาพและเคมี ได้แก่ เทคนิคการเลี้ยวเบนรังสีเอ็กซ์ การวิเคราะห์ธาตุด้วยเทคนิคเอ็กซ์อาร์  
 เอฟ การหาพื้นที่ผิวด้วยบีอีที การวิเคราะห์ด้วยกล้องจุลทรรศน์อิเล็กตรอนแบบส่องกราด การ  
 วิเคราะห์ด้วยรังสีเอ็กซ์แบบกระจายพลังงาน และการวิเคราะห์เทอร์โมแกรมเมตริก ผลการทดลอง  
 แสดงให้เห็นว่า คิวบิก  $Ce_{0.75}Zr_{0.25}O_2$  ที่มี 15 เปอร์เซ็นต์นิกเกิล ให้เกิดสังเคราะห์จาก 6.1  
 เปอร์เซ็นต์ของมีเทนคอนเวอร์ชันที่ 450 องศาเซลเซียส ในทางตรงข้าม เทตระโกนอล Ce-ZrO<sub>2</sub>  
 ( $Ce_{0.5}Zr_{0.5}O_2$  และ  $Ce_{0.15}Zr_{0.85}O_2$ ) ที่มี 15 เปอร์เซ็นต์นิกเกิลให้มีเทนคอนเวอร์ชันต่ำกว่า และมีความ  
 วงอวาระหว่างปฏิกิริยาลดลงเนื่องจากการเกิดคาร์บอน การปรับปริมาณนิกเกิลจาก 5 ถึง 20  
 เปอร์เซ็นต์ พบว่า  $Ce_{0.75}Zr_{0.25}O_2$  ที่มี 15 เปอร์เซ็นต์นิกเกิล แสดงความสามารถในการเกิดปฏิกิริยา  
 เคมีของตัวเร่งปฏิกิริยาสูงสุด จากนั้นได้ฝังรูทีเนียมปริมาณต่างๆลงบน  $Ce_{0.75}Zr_{0.25}O_2$  ที่มี 15  
 เปอร์เซ็นต์นิกเกิล ได้วิเคราะห์ความสามารถในการเกิดปฏิกิริยาเคมีของตัวเร่งปฏิกิริยาดังกล่าวใน  
 ครายรีฟอร์มมิงของมีเทน ผลการทดลองบ่งชี้ว่า 0.7 เปอร์เซ็นต์รูทีเนียมบนตัวเร่งปฏิกิริยานิกเกิล  
 ทำให้ได้ความสามารถในการเกิดปฏิกิริยาเคมีรีฟอร์มมิงสูงสุดเท่ากับ 6.9 เปอร์เซ็นต์ของมีเทนคอน  
 เวอร์ชัน สามารถสรุปได้ว่า ตัวเร่งปฏิกิริยา 15%Ni-0.7%Ru/ $Ce_{0.75}Zr_{0.25}O_2$  แสดงความสามารถใน  
 การเกิดปฏิกิริยาดีที่สุดในที่ 450 องศาเซลเซียสเป็นเวลา 17 ชั่วโมง

สถาบันวิทยบริการ  
 จุฬาลงกรณ์มหาวิทยาลัย

สาขาวิชา...ปิโตรเคมีและวิทยาศาสตร์พอลิเมอร์... ลายมือชื่อนิสิต..... ฉวาคา มาคุ่ม.....  
 ปีการศึกษา..... 2549.....ลายมือชื่ออาจารย์ที่ปรึกษา.....ศุภวรรณ ตันคยานนท์.....

# # 4772282223 : MAJOR PETROCHEMISTRY AND POLYMER SCIENCE  
 KEY WORD: DRY REFORMING OF METHANE / CERIUM ZIRCONYL OXIDE /  
 BIMETALLIC CATALYSYS

YADA MAKHUM: Ni-Ru CATALYSTS ON CERIUM ZIRCONYL OXIDE  
 FOR DRY REFORMING OF METHANE. THESIS ADVISOR:  
 ASSOC. PROF. SUPAWAN TANTAYANON, Ph. D., 68 pp.

In this research, the water-in-oil microemulsion was employed to prepare  $Ce_{1-x}Zr_xO_2$  mixed oxide which was used as a support. The impregnation method was used to impregnate 15% Ni onto the support. The ratio of  $CeO_2$  to  $ZrO_2$  was systematically varied. The prepared catalysts were characterized by various physico-chemical characterization techniques such as X-ray diffraction, X-ray fluorescence, BET surface method, Scanning Electron Microscopy, Energy Dispersive X-ray analysis, and Thermogravimetric analysis. The results showed that cubic  $Ce_{0.75}Zr_{0.25}O_2$  containing 15% Ni gave synthesis gas from 6.1% methane conversion at  $450^\circ C$ . In contrast, tetragonal Ce-ZrO<sub>2</sub> ( $Ce_{0.5}Zr_{0.5}O_2$  and  $Ce_{0.15}Zr_{0.85}O_2$ ) containing 15% Ni gave lower methane conversion and was deactivated during the reaction due to the carbon formation. By varying the amount of Ni loading from 5 to 20%, it was found that  $Ce_{0.75}Zr_{0.25}O_2$  with 15% nickel loading exhibited the highest catalytic activity. Then various amounts of Ru were impregnated onto 15% Ni/ $Ce_{0.75}Zr_{0.25}O_2$ . Their catalytic activities in dry reforming of methane were determined. The results indicated that 0.7% Ru on Ni catalyst had the highest reforming activity which was 6.9% of methane conversion. It can be concluded that 15%Ni-0.7%Ru/ $Ce_{0.75}Zr_{0.25}O_2$  catalyst exhibited the best activity in dry reforming of methane at  $450^\circ C$  for 17 h.

Field of student Petrochemistry and Polymer Science Student's signature.....*Yada Makhum*  
 Academic year .....2006..... Advisor's signature.....*Supawan Tantayanon*.....

## ACKNOWLEDGEMENTS

First of all, I would like to express my grateful appreciation to my advisor Associate Professor Supawan Tantayanon for her support, assistance, and encouragement throughout my education at Chulalongkorn University. Moreover, I would like to express my deep appreciation to Professor Pattarapan Prasassarakich, Associate Professor Wimonrat Trakarnpruk, and Assistant Professor Warinthorn Chavasiri serving as thesis committee for their valuable suggestions and comments.

I would also like to thank Sutheerawat Samingprai, my research group and my friends for standing beside me. And last but not least important, I would like to thank my parents and my brother for all the love, support, and motivation. Their encouragement and patience is greatly acknowledged.



สถาบันวิทยบริการ  
จุฬาลงกรณ์มหาวิทยาลัย

## CONTENTS

	Page
<b>ABSTRACT IN THAI</b> .....	iv
<b>ABSTRACT IN ENGLISH</b> .....	v
<b>ACKNOWLEDGEMENTS</b> .....	vi
<b>CONTENTS</b> .....	vii
<b>LIST OF TABLES</b> .....	x
<b>LIST OF FIGURES</b> .....	xi
<b>LIST OF SCHEME</b> .....	xii
<b>LIST OF ABBREVIATION</b> .....	xiii
<b>CHAPTER I INTRODUCTION</b>	
1.1 Introduction.....	1
1.2 Objective.....	2
1.3 Scope of research.....	2
<b>CHAPTER II THEORY AND LITERATURE REVIEWS</b>	
2.1 Theory.....	3
2.1.1 Dry reforming reaction .....	3
2.1.2 Characterization techniques.....	8
2.1.2.1 X-ray diffraction (XRD).....	8
2.1.2.2 Brunauer-Emmett-Teller method (BET).....	9
2.1.2.3 Scanning electron microscopy (SEM).....	9
2.1.2.4 Energy dispersive X-ray analysis (EDX).....	9
2.1.2.5 Thermogravimetric analysis (TGA).....	10
2.1.2.6 X-ray fluorescence (XRF).....	10
2.2 Literature reviews.....	11
2.2.1 Preparation of mixed cerium/zirconium oxide.....	11
2.2.2 Effect of active monometallic component.....	12
2.2.3 Effect of active bimetallic component.....	13

**CHAPTER III EXPERIMENTAL**

3.1 Materials.....	15
3.2 Equipments.....	15
3.3 Characterization methods.....	16
3.4 Experimental procedure.....	17
3.4.1 Preparation of Ce-ZrO <sub>2</sub> mixed oxides.....	17
3.4.2 Preparation of Ni/Ce-ZrO <sub>2</sub> catalysts.....	19
3.4.3 Preparation of Ru-Ni/Ce-ZrO <sub>2</sub> catalysts.....	19
3.4.4 Dry reforming reaction test.....	20
3.3.5 Instrument analysis.....	20
3.3.5.1 Determination of gas composition in dry reforming reaction by using online GC-TCD.....	20

**CHAPTER IV RESULTS AND DISCUSSION**

4.1 Preparation of Ce <sub>0.5</sub> Zr <sub>0.5</sub> O <sub>2</sub> mixed oxide.....	22
4.1.1 Proper amounts of total solid and solvent for mixed oxide preparation .....	22
4.1.2 Effect of calcination temperature .....	24
4.2 Effect of Ce <sub>1-x</sub> Zr <sub>x</sub> O <sub>2</sub> support containing 15% Ni on dry reforming.....	26
4.2.1 Preparation and characterization of Ce <sub>1-x</sub> Zr <sub>x</sub> O <sub>2</sub> support containing 15% Ni.....	26
4.2.2 Dry reforming using Ce <sub>1-x</sub> Zr <sub>x</sub> O <sub>2</sub> support containing 15% Ni....	30
4.3 Effect of Ni content of Ni catalysts on dry reforming.....	35
4.3.1 Preparation and characterization of Ni catalysts.....	35
4.3.2 Dry reforming using Ni catalysts.....	40



	Page
4.4 Effect of Ru content of Ni-Ru bimetallic catalysts on dry reforming.....	43
4.4.1 Preparation and characterization of Ni-Ru bimetallic catalysts..	43
4.4.2 Dry reforming using Ni-Ru bimetallic catalysts.....	46
<b>CHAPTER V CONCLUSIONS AND SUGGESTIONS.....</b>	<b>51</b>
<b>REFERENCES.....</b>	<b>53</b>
<b>APPENDICES.....</b>	<b>57</b>
<b>APPENDIX A.....</b>	<b>58</b>
<b>APPENDIX B.....</b>	<b>61</b>
<b>APPENDIX C.....</b>	<b>64</b>
<b>VITAE.....</b>	<b>68</b>



สถาบันวิทยบริการ  
จุฬาลงกรณ์มหาวิทยาลัย

## LIST OF TABLES

	Page
<b>Table 2.1</b> Limiting temperatures for reactions in the CO <sub>2</sub> /CH <sub>4</sub> system.....	4
<b>Table 3.1</b> Parameter used in preparation mixed oxides step.....	19
<b>Table 3.2</b> Parameter used in preparation catalysts step.....	19
<b>Table 4.1</b> The summarized parameters of Ce <sub>0.5</sub> Zr <sub>0.5</sub> O <sub>2</sub> mixed oxide by water-in-oil microemulsion method.....	23
<b>Table 4.2</b> Characteristic XRD patterns of tetragonal Ce <sub>0.5</sub> Zr <sub>0.5</sub> O <sub>2</sub> mixed oxide at different calcined temperatures.....	25
<b>Table 4.3</b> Characteristic XRD patterns of Ce <sub>1-x</sub> Zr <sub>x</sub> O <sub>2</sub> support containing 15% Ni.....	28
<b>Table 4.4</b> The XRD parameters of Ce <sub>1-x</sub> Zr <sub>x</sub> O <sub>2</sub> support containing 15% Ni.....	29
<b>Table 4.5</b> BET surface area and nickel content using XRF of Ce <sub>1-x</sub> Zr <sub>x</sub> O <sub>2</sub> support containing 15% Ni .....	30
<b>Table 4.6</b> Reaction results over Ce <sub>1-x</sub> Zr <sub>x</sub> O <sub>2</sub> support containing 15% Ni after reaction for 17 h.....	33
<b>Table 4.7</b> BET surface area of Ni catalysts.....	38
<b>Table 4.8</b> The amount of nickel content deposited on Ce <sub>0.75</sub> Zr <sub>0.25</sub> O <sub>2</sub> using XRF and EDX.....	38
<b>Table 4.9</b> Reaction results over Ni catalysts after reaction for 17 h.....	43
<b>Table 4.10</b> The crystallite size of NiO on Ni-Ru bimetallic catalysts.....	45
<b>Table 4.11</b> The BET surface area of Ni-Ru bimetallic catalysts.....	45
<b>Table 4.12</b> Ruthenium and nickel content of catalysts determined by XRF.....	46
<b>Table 4.13</b> Reaction results over Ru-Ni bimetallic catalysts.....	49

สถาบันวิทยบริการ  
 จุฬาลงกรณ์มหาวิทยาลัย

## LIST OF FIGURES

	Page
<b>Figure 2.1</b> Patterns of activation and reaction of methane with carbon dioxide on the nickel catalyst.....	8
<b>Figure 4.1</b> XRD diagrams of $Ce_{0.5}Zr_{0.5}O_2$ mixed oxide synthesized with different amounts of solid and solvent after calcined in air at $500^\circ C$ for 5 h using a ramp of $4^\circ Cmin^{-1}$ .....	23
<b>Figure 4.2</b> XRD diagrams of $Ce_{0.5}Zr_{0.5}O_2$ at different calcination temperatures.....	24
<b>Figure 4.3</b> XRD diagrams of $Ce_{1-x}Zr_xO_2$ support containing 15% Ni: (a) Ni/ $CeO_2$ , (b) Ni/ $Ce_{0.75}Zr_{0.25}O_2$ , (c) Ni/ $Ce_{0.5}Zr_{0.5}O_2$ , (d) Ni/ $Ce_{0.15}Zr_{0.85}O_2$ and (e) Ni/ $ZrO_2$ .....	27
<b>Figure 4.4</b> $CH_4$ and $CO_2$ conversions with time on stream over $Ce_{1-x}Zr_xO_2$ support containing 15% Ni (reaction condition: $T = 450^\circ C$ , $CH_4/CO_2 = 1 : 1$ ): (a) Ni/ $CeO_2$ , (b) Ni/ $Ce_{0.75}Zr_{0.25}O_2$ , (c) Ni/ $Ce_{0.5}Zr_{0.5}O_2$ , (d) Ni/ $Ce_{0.15}Zr_{0.85}O_2$ and (e) Ni/ $ZrO_2$ .....	31
<b>Figure 4.5</b> CO yield with time on stream over $Ce_{1-x}Zr_xO_2$ support containing 15% Ni (reaction condition: $T = 450^\circ C$ , $CH_4/CO_2 = 1 : 1$ ): (a) Ni/ $CeO_2$ , (b) Ni/ $Ce_{0.75}Zr_{0.25}O_2$ , (c) Ni/ $Ce_{0.5}Zr_{0.5}O_2$ , (d) Ni/ $Ce_{0.15}Zr_{0.85}O_2$ and (e) Ni/ $ZrO_2$ .....	32
<b>Figure 4.6</b> SEM images of Ni/ $Ce_{0.75}Zr_{0.25}O_2$ catalyst: (a) before the reaction, and (b) after the reaction for 17 h at $450^\circ C$ .....	34
<b>Figure 4.7</b> XRD patterns of Ni catalysts at different nickel loading: (a) 20% Ni, (b) 15% Ni, (c) 10% Ni, and (d) 5% Ni.....	36
<b>Figure 4.8</b> EDX mapping of Ni catalysts: (a) 5% Ni, (b) 10% Ni, (c) 15% Ni, and (d) 20% Ni.....	39
<b>Figure 4.9</b> $CH_4$ and $CO_2$ conversions with time on steam over Ni catalysts in dry reforming of methane (reaction condition: $T = 450^\circ C$ , $CH_4/CO_2 = 1 : 1$ ).....	41
<b>Figure 4.10</b> CO yield with time on stream over Ni catalysts in dry reforming of methane (reaction condition: $T = 450^\circ C$ , $CH_4/CO_2 = 1 : 1$ ).....	42
<b>Figure 4.11</b> XRD patterns of Ni-Ru catalyst with various ruthenium loadings.....	44
<b>Figure 4.12</b> $CH_4$ and $CO_2$ conversions with time on steam over Ru on Ni catalysts in dry reforming of methane (reaction condition: $T = 450^\circ C$ , $CH_4/CO_2 = 1 : 1$ ).....	47
<b>Figure 4.13</b> CO and $H_2$ yields with time on stream over Ru on Ni catalysts in dry reforming of methane (reaction condition: $T = 450^\circ C$ , $CH_4/CO_2 = 1 : 1$ ).....	48

## LIST OF SCHEME

Page

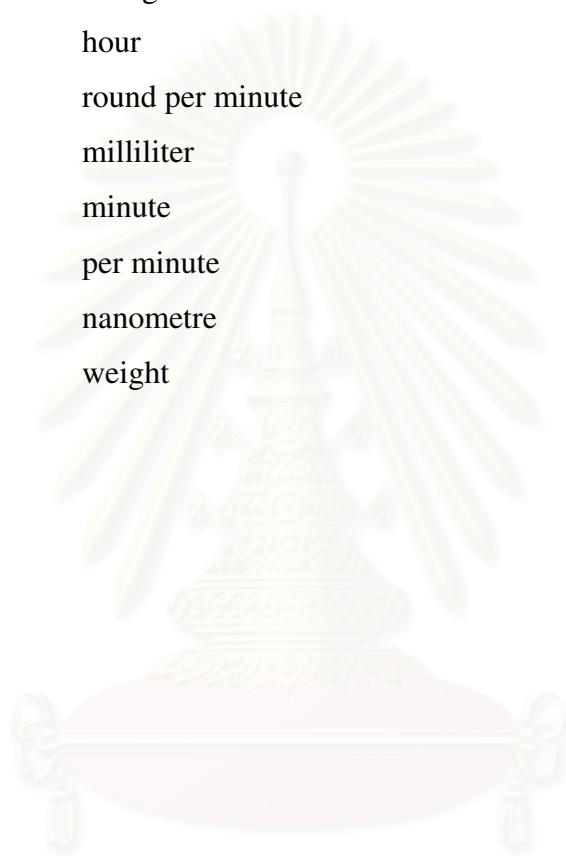
<b>Scheme 3.1</b> Preparation of Ce-ZrO <sub>2</sub> mixed oxide.....	18
---	----



สถาบันวิทยบริการ  
จุฬาลงกรณ์มหาวิทยาลัย

**LIST OF ABBREVIATION**

T	temperature
°C	degree Celsius
atm	atmosphere
g	gram
mg	milligram
h	hour
rpm	round per minute
ml	milliliter
min	minute
min <sup>-1</sup>	per minute
nm	nanometre
wt	weight



สถาบันวิทยบริการ  
จุฬาลงกรณ์มหาวิทยาลัย

# CHAPTER I

## INTRODUCTION

### 1.1 Introduction

Recently, dry reforming of methane for production of synthesis gas is becoming an attractive for the chemical utilization of natural gas and carbon dioxide which is substances intimately related to greenhouse effect and energy resources. Numerous supported catalysts have been tested especially nickel and noble metal-based catalysts [1].

Supported-Ni catalysts have been tried for this reaction and showed high activity comparable to noble metals [2]. However, the coke formation over nickel-based catalysts during the dry reforming is known to be more serious than for any other reforming reactions. It is well known that bimetallic catalysts exhibit superior activity, selectivity and deactivation resistance than the corresponding monometallic samples [3].

There has been a lot recent interest in mixed oxide catalyst systems like  $Ce_{1-x}Zr_xO_2$  (Ce-ZrO<sub>2</sub>) because of certain inherent advantages [4]. Moreover, it has been reported that the nature of supports affects the catalytic performance of Ni catalysts in dry reforming of methane. The activity and stability of these catalysts varied greatly with different supports. It is known that the addition of ZrO<sub>2</sub> to CeO<sub>2</sub> leads to improvements in oxygen storage capacity of CeO<sub>2</sub>, redox property, thermal resistance and promotion of metal dispersion [5]. Furthermore, it has been established that the reducibility of CeO<sub>2</sub> is greatly enhanced when it is mixed with ZrO<sub>2</sub> to form a solid solution of  $Ce_{1-x}Zr_xO_2$ . Therefore, the Ce-ZrO<sub>2</sub> system has appeared as a promising candidate of a support material in bimetallic catalyst system.

## 1.2 Objective

1. To synthesize the Ni-Ru/Ce<sub>1-x</sub>Zr<sub>x</sub>O<sub>2</sub> bimetallic catalysts.
2. To optimize the bimetallic catalyst in dry reforming of methane at 450°C for 17h.

## 1.3 Scope of research

### 1.3.1 Survey literature

### 1.3.2 Synthesize Ce-ZrO<sub>2</sub> mixed oxides by water-in-oil microemulsion method

### 1.3.3 Synthesize Ni/Ce-ZrO<sub>2</sub> catalyst by the impregnation method

### 1.3.4 Synthesize Ru-Ni/Ce-ZrO<sub>2</sub> catalyst by the impregnation method

### 1.3.5 Characterize the prepared catalysts by following methods:

- X-ray diffraction (XRD)
- X-ray fluorescence (XRF)
- Brunauer-Emmett-Teller method (BET)
- Scanning electron microscopy (SEM)
- Energy dispersive X-ray analysis (EDX)
- Thermogravimetric analysis (TGA)
- Gas Chromatography (GC)

### 1.3.5 Summarize the results and write thesis

## CHAPTER II

### THEORY AND LITERATURE REVIEWS

#### 2.1 Theory

##### 2.1.1 Dry reforming reaction

The thermodynamics of the carbon dioxide reforming of methane has been deeply investigated. The corresponding carbon dioxide reforming reaction is described as



This reaction is highly endothermic and equally favored by low pressure but requires a higher temperature. A reverse water-gas shift reaction occurs as a side reaction:



Under conditions of stoichiometric  $\text{CO}_2$  reforming, carbon depositions occurs as in the Boudouard reaction



and in the methane cracking





The standard free energy change employed to calculate the minimum operation temperatures for CO<sub>2</sub> reforming and CH<sub>4</sub> cracking, and the upper limiting temperatures of the other side reaction (2.2) and (2.3). Assuming  $\Delta G^\circ = 0$ , the upper or lower limiting temperatures for reactions (2.1) - (2.4) will be obtained. CO<sub>2</sub>/CH<sub>4</sub> reaction can proceed above 645°C accompanied by methane cracking reaction, while above 817°C reverse water gas shift reaction and the Boudouard reaction could not occur. In the temperature range of 557~700°C carbon will form from methane cracking of the Boudouard reaction.

**Table 2.1** Limiting temperatures for reactions in the CO<sub>2</sub>/CH<sub>4</sub> system

	<b>Reaction</b>			
	<b>1<sup>a</sup></b>	<b>2<sup>b</sup></b>	<b>3<sup>b</sup></b>	<b>4<sup>a</sup></b>
<b>Temperature /°C</b>	645	817	700	557
<b>Reaction type</b>	Reforming	RWGS	CO → C	CH <sub>4</sub> cracking
<b>Reaction taking place</b>	≥645	≤817	≤700	≥557

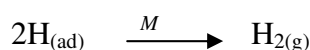
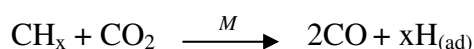
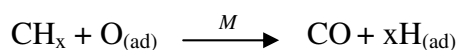
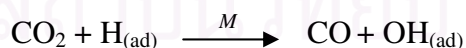
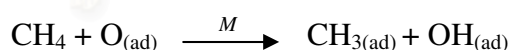
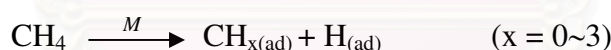
*a: Lower limit and b: Upper limit*

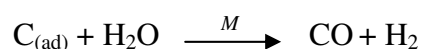
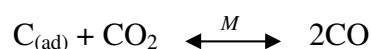
Nowadays, two viewpoints have been proposed about the mechanism of dry reforming of methane. The general opinion is that firstly methane is adsorbed, activated and dissociated on the reduced metal catalyst. Nevertheless, the divarication occurs about whether carbon dioxide also dissociate on the surface of the catalyst. Takayasu [6] suggested that gaseous carbon dioxide directly reacted with hydrogen formed from methane to water, steam reforming then followed to obtain synthesis gas. That is to say, the substance of the carbon dioxide reforming is the same as the steam reforming.

The reaction of methyl species on Ni(111) and Ni(110) was studied [7] employing mass spectroscopy. The results showed that the C-H rupture of methyl readily occurs at  $-53.15^{\circ}\text{C}$ . It gave good evidence that C-H rupture of fairly stable methyl is easy. The activation of methane on VIII group metals is not very difficult. The strong chemisorption of  $\text{CH}_x$  and hydrogen formed by methane on metals may largely decreased the energy barrier of dehydrogenation of methane and promotes the stepwise dissociation at lower temperature. Compared with VIII group metals, the metal oxide catalysts have not the strong interaction with methane and  $\text{CH}_x$ . So, the very high temperature is necessary for the activation of methane to supply enough energy.

Erdohelyi *et al.* [8] proposed the mechanism of dry reforming of methane over supported noble metal catalysts on the basis of kinetic studies. Methane may undergo two reactions as following routes: stepwise dehydrogenation followed by the surface reaction with surface oxygen or OH to CO and  $\text{H}_2$  (1), or direct reaction with surface oxygen species to  $\text{CH}_x$  then follow former route (2). Carbon dioxide may react with adsorbed hydrogen, surface carbon and surface  $\text{CH}_x$  fragments.

The proposed mechanism is as follows:





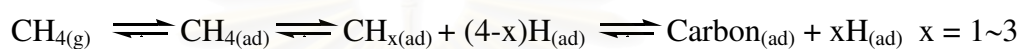
The mechanism of dry reforming of methane may somewhat change when different type of catalysts are used. Zhang *et al.* [9] reported that Ni/La<sub>2</sub>O<sub>3</sub> catalyst showed high stability because a new reaction pathway occurred at the Ni/La<sub>2</sub>O<sub>3</sub> interface. They proposed a mechanism that under the CO<sub>2</sub>/CH<sub>4</sub> reaction conditions, CH<sub>4</sub> mainly cracks on the Ni crystallites to form H<sub>2</sub> and surface carbon species (CH<sub>x</sub> species), while CO<sub>2</sub> is preferably adsorbed on the Ni/La<sub>2</sub>O<sub>3</sub> support or the LaO<sub>x</sub> species which are decorating the Ni crystallites in the form of La<sub>2</sub>O<sub>2</sub>CO<sub>3</sub>. At high temperatures the oxygen species of La<sub>2</sub>O<sub>2</sub>CO<sub>3</sub> may participate in the reactions with the surface carbon species (CH<sub>x</sub>) on the neighboring Ni sites to form CO. Owing to the existence of such synergetic sites which consist of Ni and La elements, the carbon species formed on the Ni sites are favorably removed by the oxygen species originated from La<sub>2</sub>O<sub>2</sub>CO<sub>3</sub>, thus resulting in an active and stable performance.

Yan *et al.* [10] reported that the decomposition of methane on nickel catalyst could result in the formation of at least three kinds of surface carbon species on supported nickel catalyst. Generally, the carbon deposition comprises various forms of carbon which are different in terms of reactivity. The distribution and features of these carbonaceous species depend sensitively on the nature of transition metals and the conditions of methane adsorption. These carbonaceous species can be described as: completely dehydrogenated carbidic C<sub>∞</sub> type, partially dehydrogenated CH<sub>x</sub> (1 ≤ x ≤ 3) species, namely C<sub>β</sub> type, and carbidic cluster C<sub>γ</sub> type formed by the agglomeration and conversion of C<sub>∞</sub> and C<sub>β</sub> species under certain conditions. A fraction of the surface carbon species, which might be assigned to carbidic C<sub>∞</sub> (~188°C), was mainly hydrogenated to methane even below 227°C. It showed that carbidic C<sub>∞</sub> species is rather active and thermally unstable on nickel surface. The carbidic C<sub>∞</sub> species was suggested to be responsible for CO formation. A significant amount of surface carbon species were hydrogenated to methane below 327°C and were assigned to partially dehydrogenated C<sub>β</sub> (~310°C) species. The majority of the

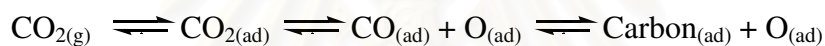
surface carbon was hydrogenated above 527°C and was attributed to carbidic clusters  $C_\gamma$  (~550°C). The possible reaction processes of carbon dioxide reforming with methane was inferred as follows: methane is firstly decomposed into hydrogen and different surface carbon species, then the adsorbed  $CO_2$  reacts with surface carbons to form CO.

The proposed mechanism is as follows [10].

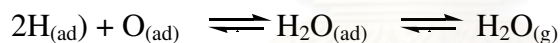
1) Dissociative adsorption of methane is the rate-determining step.



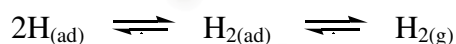
2) Dissociative adsorption of carbon dioxide



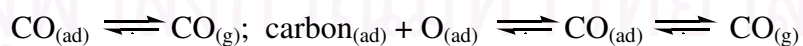
3) Formation of water



4) Formation of hydrogen



5) Formation of carbon monoxide and decarbonation



This mechanism is actually the synergic decomposition process of methane and carbon dioxide (described as Figure 2.1)

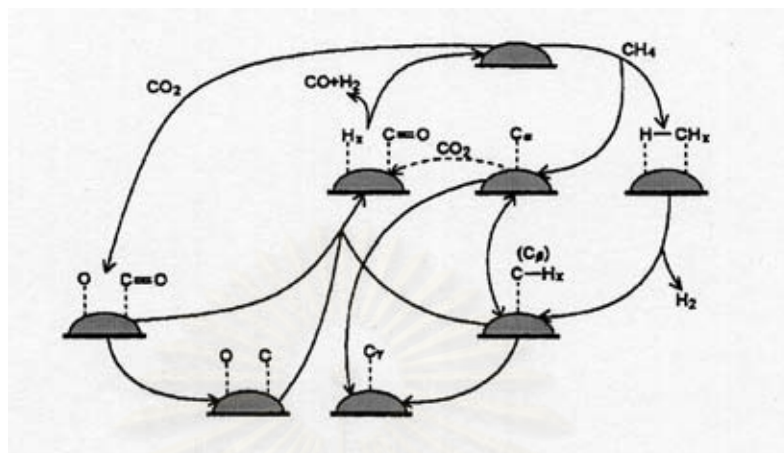


**Figure 2.1** Patterns of activation and reaction of methane with carbon dioxide on the nickel catalyst.

## 2.1.2 Characterization Techniques

### 2.1.2.1 X-ray diffraction (XRD)

X-ray Powder Diffraction (XRD) is an efficient analytical technique used to identify and characterize unknown crystalline materials. Monochromatic x-rays are used to determine the interplanar spacings of the unknown materials. Samples are analyzed as powders with grains in random orientations to insure that all crystallographic directions are "sampled" by the beam. When the Bragg conditions for constructive interference are obtained, a "reflection" is produced, and the relative peak height is generally proportional to the number of grains in a preferred orientation. The x-ray spectra generated by this technique, thus, provide a structural fingerprint of the unknown. Mixtures of crystalline materials can also be analyzed and relative peak heights of multiple materials may be used to obtain semi-quantitative estimates of abundances. A glancing x-ray beam may also be used to obtain structural information of thin films on surfaces. In addition, changes in peak position that represent either compositional variation (solid solution) or structure-state information (e.g. order-

disorder transitions, etc.) are readily detectable. Peak positions are reproducible to 0.02 degrees.

#### **2.1.2.2 Brunauer-Emmett-Teller method (BET)**

BET theory is a well-known rule for the physical adsorption of gas molecules on a solid surface. The concept of the theory is an extension of the Langmuir theory, which is a theory for monolayer molecular adsorption, to multilayer adsorption with the following hypotheses: (a) gas molecules physically adsorb on a solid in layers infinitely; (b) there is no interaction between each adsorption layer; and (c) the Langmuir theory can be applied to each layer.

#### **2.1.2.3 Scanning electron microscopy (SEM)**

The imaging method of the scanning electron microscope (SEM) allows separation of the two functions of a microscope, localization and information transfer. The SEM utilizes a very fine probing beam of electrons which sweeps over the specimen to emit a variety of radiations. The signal, which is proportional to the amount of radiation leaving an individual point of the specimen at any instant, can be used to modulate the brightness of the beam of the display cathode-ray tube as it rests on the corresponding point of the image. In practice, the points follow one another with great rapidity so that the image of each point becomes an image of a line, and the line in turn can move down the screen so rapidly that the human eye sees a complete image as in television. The image can also be recorded in its entirety by allowing the point-by-point information to build up in sequence on a photographic film.

#### **2.1.2.4 Energy dispersive X-ray analysis (EDX)**

An energy-dispersive x-ray analyzer (EDX) is a common accessory which gives the scanning electron microscope (SEM) a very valuable capability for elemental analysis. The electron beam in an SEM has an energy typically between 5,000 and 20,000 electron volts (eV). The energy holding electrons in atoms (the binding energy) ranges from a few eV up to many kilovolts. Many of these atomic

electrons are dislodged as the incident electrons pass through the specimen, thus ionizing atoms of the specimen. Ejection of an atomic electron by an electron in the beam ionizes the atom, which is then quickly neutralized by other electrons. In the neutralization process an x-ray with an energy characteristic of the parent atom is emitted. By collecting and analyzing the energy of these x-rays, the constituent elements of the specimen can be determined.

#### **2.1.2.5 Thermogravimetric analysis (TGA)**

Thermogravimetry (TG) provides the analyst with quantitative measurement of any weight change associated with a transition. For example, TG can directly record the loss in weight with time or temperature due to dehydration or decomposition. Thermogravimetric curves are characteristic for a given compound or system because of the unique sequence of physicochemical reactions which occur over definite temperature ranges and at rates that are a function of the molecular structure. Changes in weight are a result of the rupture and/or formation of various physical and chemical bonds at elevated temperature that lead to the evolution of volatile products or the formation of heavier reaction products. From such curves data are obtained concerning the thermodynamics and kinetics of the various chemical reactions, reaction mechanisms, and the intermediate and final reaction products. The usual temperature range is from ambient to 1200°C with inert or reactive atmosphere.

#### **2.1.2.6 X-ray fluorescence (XRF)**

X-Ray fluorescence (XRF) is a quantitative elemental analysis technique based on the characteristic X-ray emission behavior of different elements under incident X-ray irradiation. When supplied with high energy radiation (e.g. X-ray), an electron is knocked out of its shell, and replaced with an electron from a higher energy shell. This high-low energy transition results in the emission of photons, the set of wavelengths for which is specific to each element. Examination of relative intensities of different emitted wavelengths can thus give a quantitative measurement of relative quantities of each element in a sample.

## 2.2 Literature reviews

### 2.2.1 Preparation of mixed cerium/zirconium oxide

In 2000, Montoya *et al.* [5] studied Ni/ZrO<sub>2</sub> catalysts promoted with different amounts of CeO<sub>2</sub> (0, 1, 8 and 20 %wt.) which were prepared by the sol-gel method. The increasing of CeO<sub>2</sub> concentration led to increase both of t-ZrO<sub>2</sub> stability and catalyst activity, although some degree of deactivation, due mainly to the sintering of the support, was not completely avoided by ceria addition. CeO<sub>2</sub> also induced a larger difference between CO<sub>2</sub> and CH<sub>4</sub> conversions and a lowering of the H<sub>2</sub>/CO ratio, thus enhancing the reverse water gas shift reaction during dry reforming of methane

In 2003, Menad *et al.* [4] prepared a novel Ru/Ce<sub>0.5</sub>Zr<sub>0.5</sub>O<sub>2</sub> catalyst by the impregnation with Ru<sup>3+</sup> of a mixed Ce-Zr oxide obtained by water-in-oil microemulsion method. Under reaction condition (T = 650°C, 19h), the catalyst supported on Zr and Ce oxides prepared by the microemulsion method showed higher activity and stability than prepared by the impregnation which including single oxides (CeO<sub>2</sub>, ZrO<sub>2</sub>, and SiO<sub>2</sub>) and CeO<sub>2</sub>-ZrO<sub>2</sub> mixed oxides. Only 3% activity was lost within the first 8 h in reaction and its performance was perfectly maintained for a further 12 h. The introduction of cerium as a promoter in the ZrO<sub>2</sub> structures was shown to improve the catalyst performance by increasing the oxygen mobility in the support and consequently reducing deactivation by carbon deposition during reaction.

In 2004, Roh *et al.* [11] used the co-precipitation method to prepare nickel oxide dispersed on CeO<sub>2</sub>, ZrO<sub>2</sub> and cubic Ce<sub>0.8</sub>Zr<sub>0.2</sub>O<sub>2</sub> support compared with the conventional impregnation method for dry reforming of methane reaction. The co-precipitated Ni-Ce-ZrO<sub>2</sub> catalyst had higher BET surface area, smaller nanocrystallite sizes of both Ce<sub>0.8</sub>Zr<sub>0.2</sub>O<sub>2</sub> support and NiO compared with the impregnated one. The co-precipitated Ni-Ce-ZrO<sub>2</sub> catalyst also exhibited high activity and stability during reaction at 800°C.



In 2004, Kuznetsova *et al.* [12] reported that the surface and bulk oxygen reactivity and mobility of ceria-based solid solutions as related to the process of methane conversion into syngas can be tuned in a broad limits by bulk and surface promoters. Results of TPR experiments with different reductants reasonably agree as far as the effect of ceria-based solid solutions doping on the reactivity of the surface/bulk oxygen and its amount was concerned.

In 2004, Xiancai *et al.* [13] studied the catalytic activity and coke resistance of  $\text{La}_2\text{O}_3$  promoted nickel-based catalysts. Catalysts were characterized by CO-TPD,  $\text{CO}_2$ -TPD, TPR, XPS and XRD techniques. They found that the catalytic activity, resistance to carbon deposition and the stability of the catalysts can be greatly improved with the addition of a rare earth oxide. Compared with the catalyst prepared by impregnation method, rare earth-doped Ni-based catalyst prepared by sol-gel procedure has more oxygen vacancies, led to higher catalytic activity. Thus 5.0 %wt. Ni-0.75%wt. La-BaTiO<sub>3</sub> shows higher catalytic activity than the catalysts 5.0%wt. Ni/La-BaTiO<sub>3</sub> (Ba/La = 1/0.002) and 5.0 %wt. Ni-1.5 %wt. La/BaTiO<sub>3</sub>.

In 2005, Laosiripojana *et al.* [14] reported that doping of CeO<sub>2</sub> on Ni/Al<sub>2</sub>O<sub>3</sub> was improved dry reforming activity for H<sub>2</sub> and CO productions at solid oxide fuel cell (SOFC) operating temperature 800-900°C. In particular, 8% CeO<sub>2</sub> doped Ni/Al<sub>2</sub>O<sub>3</sub> showed the best reforming reactivity among those with ceria content in the range of 0 to 14 %wt.

### 2.2.2 Effect of active monometallic component

In 2002, Dong *et al.* [15] studied the effect of Ni content on the Ni/Ce-ZrO<sub>2</sub> catalyst for oxy-reforming, steam reforming and oxy-steam reforming. Among the various values of Ni loading (3-30 %wt.), the conversion of methane in all the reactions increased with increasing nickel content up to 15 %wt. and then decreased above this value. The 15 %wt. Ni/Ce-ZrO<sub>2</sub> exhibited not only the highest catalytic activity and selectivity but also remarkable stability.

In 2005, Schulz *et al.* [16], reported that a Pd/ $\alpha$ -Al<sub>2</sub>O<sub>3</sub> catalyst with a low metal loading close to 1% exhibited a catalytic activity for dry reforming of methane above 600°C comparable to those of similar Pt or Rh catalysts. The decline in activity was due to palladium sintering. The addition of Ce to Pd/ $\alpha$ -Al<sub>2</sub>O<sub>3</sub> practically eliminated the deposition of carbon and diminished the sintering process, increasing the stability of the catalyst for the reforming reaction.

In 2006, Chang *et al.* [17] prepared zirconia-supported nickel catalysts by an incipient wetness method. Among nickel content of 2.5-23 %wt., 13 %wt. Ni/ZrO<sub>2</sub> catalyst exhibited the highest activity. Moreover, Ni/ZrO<sub>2</sub> with a Ce modifier and a Ca promoter prepared by sol-gel method and impregnation of metal led to higher activity as well as catalyst stability.

In 2006, Pompeo *et al.* [18] studied Ni and Pt catalysts supported on  $\alpha$ -Al<sub>2</sub>O<sub>3</sub>,  $\alpha$ -Al<sub>2</sub>O<sub>3</sub>-ZrO<sub>2</sub> and ZrO<sub>2</sub> in dry reforming of methane. It was found that 2 %wt. Ni based catalysts were more active than 1 %wt. Pt based catalysts. The lowest deactivation observed in Ni and Pt support on  $\alpha$ -Al<sub>2</sub>O<sub>3</sub>-ZrO<sub>2</sub>, compared to  $\alpha$ -Al<sub>2</sub>O<sub>3</sub> can be explained by an inhibition of carbon deposition in system having ZrO<sub>2</sub>.

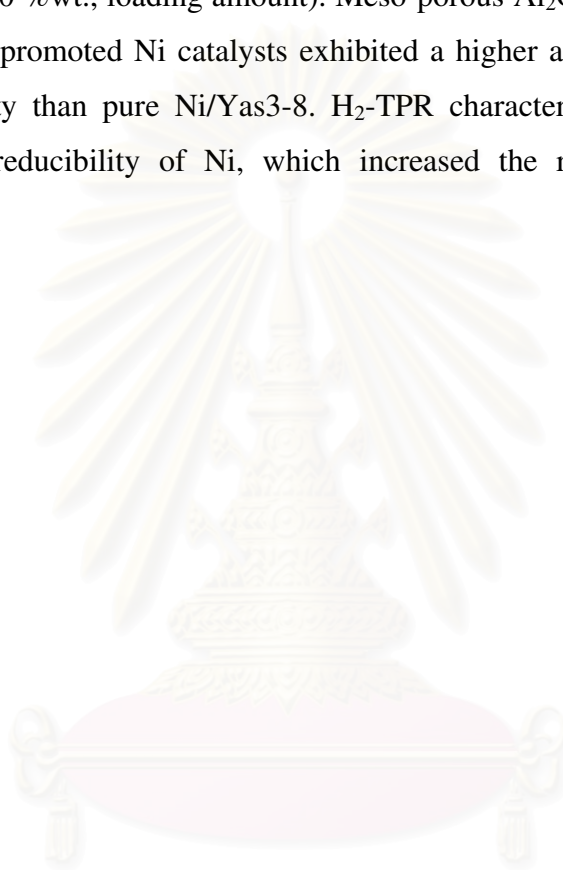
### **2.2.3 Effect of active bimetallic component**

In 2005, Jozwiak *et al.* [19] studied the activity and stability of silica supported monometallic Ni, Rh and bimetallic Ni-Rh catalysts towards the dry reforming of methane. The results showed that both monometallic and bimetallic were comparably good catalyst for this reaction and Rh-rich catalysts are resistant to deactivation and carbon formation. For bimetallic 2.5 %wt.Ni-2.5%wt. Rh/SiO<sub>2</sub> prepared by incipient wetness method showed the 82% CH<sub>4</sub> conversion at 700°C with the loss of activity about 1.6% and 3.6% of coke formation.

In 2002, Crisafulli *et al.* [3] reported about the effect of addition of Ru to supported Ni catalysts towards the dry reforming of methane. The increasing of Ru content led to both activity and stability increased. The influence of Ru addition was instead much less remarkable on H-ZSM5 zeolite than silica supported samples. They

suggested that the Ni-Ru interaction observed over H-ZSM5 zeolite supported catalysts was lower than over silica. Therefore, a 1.94 %wt.Ni-0.63 %wt.Ru/silica gave the higher strong improvement in the activity and stability.

In 2006, Hou *et al.* [2] reported that the noble metals (5 %wt. Ru, Rh, Pt, Pd, and Ir) showed higher coke resistance ability, while their activity was lower than that of Ni and Co (10 %wt., loading amount). Meso-porous Al<sub>2</sub>O<sub>3</sub> supported Rh and small amounts of Rh-promoted Ni catalysts exhibited a higher activity and excellent coke resistance ability than pure Ni/Yas3-8. H<sub>2</sub>-TPR characterization indicated that Rh improved the reducibility of Ni, which increased the reforming activity of the catalysts.



สถาบันวิทยบริการ  
จุฬาลงกรณ์มหาวิทยาลัย

# CHAPTER III

## EXPERIMENTAL

### 3.1 Materials

1. Zirconyl nitrate ( $\text{ZrO}(\text{NO}_3)_2 \cdot \text{H}_2\text{O}$ ), Acros
2. Cerium nitrate hexahydrate ( $\text{Ce}(\text{NO}_3)_2 \cdot 6\text{H}_2\text{O}$ ), Acros
3. Heptane ( $\text{n-C}_7\text{H}_{16}$ ), Carlo
4. Hexanol ( $\text{n-C}_6\text{H}_{14}\text{O}$ ), Acros
5. t-Octylphenoxypolyethoxyethanal (Triton X-100), Acros
6. Tetramethylammonium hydroxide ( $(\text{CH}_3)_4\text{NOH}$ ), Fluka
7. Nickel nitrate hexahydrate ( $\text{Ni}(\text{NO}_3)_2 \cdot 6\text{H}_2\text{O}$ ), Carlo
8. Ruthenium (III) nitrosyl nitrate, Aldrich
9. Methyl alcohol, Carlo
10. Quartz wool, Alltech
11. Helium gas, Bangkok Industrial Gas Co., Ltd. (BIG)
12. Argon gas, Thai Industrial Gas Co., Ltd. (TIG)
13. Hydrogen gas, Bangkok Industrial Gas Co., Ltd. (BIG)
14. Standard hydrogen in argon, Thai Industrial Gas Co., Ltd. (TIG)
15. Standard mixed gas, methane: carbon dioxide (1:1), Bangkok Industrial Gas Co., Ltd. (BIG)

### 3.2 Equipments

1. Oven, Memmert UM-500
2. Furnace, Carbolite RHF 1600 muffle furnace
3. Home-made reaction apparatus
4. Digital flow meter, Alltech
5. Flow meter

### 3.3 Characterization methods

#### **X-ray powder diffraction (XRD)**

The X-ray diffraction (XRD) patterns were recorded using a D/Max 2002 Rigaku diffractometer using Cu K $\alpha$  radiation. X-ray diffraction was used to obtain information of the structure and composition.

#### **Brunauer-Emmett-Teller method (BET)**

The surface area was measured by nitrogen adsorption at -196°C using a BELSORP-mini. The BET surface area was determined by N<sub>2</sub> adsorption which decreases with increasing particle size. The quantity of adsorbed material gave directly the total surface area of the sample which based upon on adsorbed.

#### **Scanning Electron Microscopy (SEM)**

The morphology of catalysts were observed by scanning electron microscope (SEM) using JEOL model JSM-5800 LV with electro dispersive spectrometer (EDS) for qualitative and quantitative analysis. The spatial resolution for SEM-EDX lies between 0.8 and 1.2  $\mu\text{m}$  for the samples we investigated. For avoid charging, prior SEM analysis sample was painted with carbon ink and gold-coated.

#### **Thermogravimetric Analyzer (TGA)**

Thermogravimetric analyses (TGA) of carbon deposition and removal were performed on at atmospheric pressure. The weight change over specific temperature ranges provides indications of the composition of the sample and thermal stability. Each catalyst sample (about 20 mg) was heated from 30 to 800 °C at a rate of 20°Cmin<sup>-1</sup> in the flow (58 mlmin<sup>-1</sup>) of N<sub>2</sub>, and holding for 10 min. At 800°C, the run was continued for 30 min in air 8 mlmin<sup>-1</sup> with N<sub>2</sub> 50 mlmin<sup>-1</sup> for 20 min.

## **X-ray fluorescence (XRF)**

The weight content of metal loadings was determined by X-ray fluorescence (XRF) analysis using WD-XRF model PW-2400.

## **3.4 Experimental procedure**

In this chapter the experimental procedure was divided into 5 parts

3.4.1 Preparation of Ce/ZrO<sub>2</sub> mixed oxides

3.4.2 Preparation of Ni-Ce/ZrO<sub>2</sub> catalysts

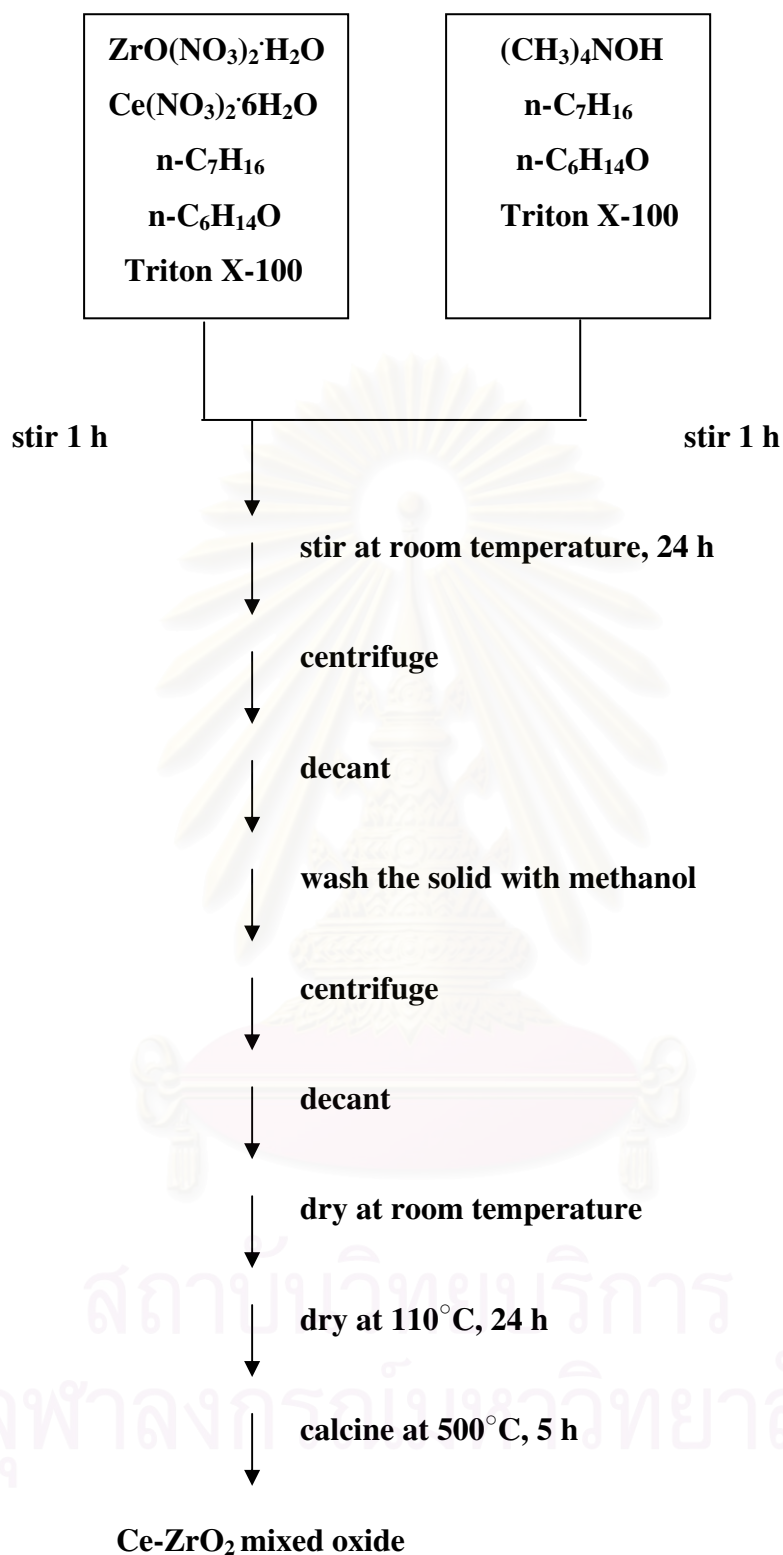
3.4.3 Preparation of Ru-Ni-Ce/ZrO<sub>2</sub> catalysts

3.4.4 Dry reforming reaction test

3.3.5 Instrument analysis

### **3.4.1 Preparation of Ce-ZrO<sub>2</sub> mixed oxides**

Zr-Ce mixed oxide was prepared by the microemulsion method. To synthesize the support, a water-in-oil microemulsion was prepared by mixing, while stirring 50 ml of an aqueous solution containing the same concentration (0.25 M) of both Zr and Ce ions (zirconyl nitrate (ZrO(NO<sub>3</sub>)<sub>2</sub>·H<sub>2</sub>O) and cerium nitrate hexahydrate (Ce(NO<sub>3</sub>)<sub>2</sub>·6H<sub>2</sub>O) with 427 ml of heptane (n-C<sub>7</sub>H<sub>16</sub>), 92.8 ml of hexanol (n-C<sub>6</sub>H<sub>14</sub>O) and 88.8 ml of surfactant (Triton X-100). Another similar WO microemulsion was prepared with containing tetramethylammonium hydroxide ((CH<sub>3</sub>)<sub>4</sub>NOH) as an aqueous solution. After stirred separately for 1 h, then mixed and stirred at room temperature for 24 h. The resulting suspension was centrifuged for 20 min with 6,000 rpm, decanted and washed the remaining solid with methanol. After centrifuging and decanting again, the solid was first dried for a 15 min. at room temperature, then at 110°C for 24 h and finally it was calcined in air at 500°C for 5 h using a ramp of 4°Cmin<sup>-1</sup>. In this step, the consider parameters were shown in Table 3.1.



**Scheme 3.1** Preparation of Ce-ZrO<sub>2</sub> mixed oxide.

**Table 3.1** Parameter used in preparation mixed oxides step.

Weight of total solid (g)	0.0145, 0.7250, 1.0875, 1.4500
Calcination temperature (°C)	500-900

### 3.4.2 Preparation of Ni/Ce-ZrO<sub>2</sub> catalysts

Supported catalysts with Ni loadings of 5-20% wt was prepared on the diverse supports by the impregnation method using nickel nitrate hexahydrate (Ni(NO<sub>3</sub>)<sub>2</sub>·6H<sub>2</sub>O). The impregnated catalysts were first dried for 15 min at room temperature, and then at 110°C for 24 h and finally it was calcined in air at 800°C for 5 h using a ramp of 4°Cmin<sup>-1</sup>. In this step, the consider parameters were shown in Table 3.2

**Table 3.2** Parameter used in preparation catalysts step.

Ce/Zr ratio	0.15, 0.5, 0.75, 1
Ni (% wt.)	5, 10, 15, 20

### 3.4.3 Preparation of Ru-Ni/Ce-ZrO<sub>2</sub> catalysts

The impregnation method using nickel nitrate hexahydrate (Ni(NO<sub>3</sub>)<sub>2</sub>·6H<sub>2</sub>O) and ruthenium (III) nitrosyl nitrate, Aldrich), respectively for impregnating to the supports. Then, the catalysts were dried for 15 min at room temperature, then at 110°C for 24 h and finally it were calcined in air at 800°C for 5 h using a ramp of 4°Cmin<sup>-1</sup>.



### **3.4.4 Dry reforming reaction test**

The catalytic activity was carried out using a fixed-bed reactor at atmospheric pressure in dry reforming of methane. Each catalyst of 1.0 g was loaded in the shell side by using two quartz wool plugs at both ends of the shell side of the reactor. The catalyst was reduced in the reactor with pure hydrogen gas 20 ml/min at 550°C for 4 h prior to each catalytic measurement at atmospheric pressure. Helium or argon gas was flushed and used as a carrier gas for the entire experiment. The reactant feed comprised a gaseous mixture of CH<sub>4</sub>:CO<sub>2</sub> (1:1) were introduced into reactor controlled by a mass flow controller and the flow rate was controlled at 20 ml/min. The pressure of the feed gas was monitored by a pressure gauge. Temperature controllers (Omega CN-9000) were used to control the temperature of the furnace and the reactor. A thermocouple was placed inside the tube side in order to control the temperature in the catalytic bed. The catalyst lifetime of dry reforming reaction test was preformed for 17 h at temperature 450°C and was monitored by using on-line gas chromatography.

### **3.3.5 Instrument analysis**

#### **3.3.5.1 Determination of gas composition in dry reforming reaction by using online GC-TCD**

The gas composition from the shell side were analyzed by the on-line gas chromatography (Perichrom model PR2100) equipped with two automotive valves, a sampling valve and a bypass valve. The Clarity computer software was used for acquiring and analyzing the all data. A serial/bypass configuration was arranged for two isothermal columns; Hayesep Q (no.1) and Molecular sieve 13X (no.2), at 40°C. The valve no.2 was set to “off” during the entire experiment. While the valve no.1 was set to “on” for 19 seconds and then “off”. To allow injection of sample gases, the carrier gas with pressure 150kPa directed the mixture of methane, carbon monoxide, carbon dioxide, and hydrogen went through the Heyasep Q column, and then quickly entered the serial-arranged Molecular sieve 13X for separating the hydrogen and carbon monoxide, where those gases were separated and passed to the Thermal Conductivity Detector (TCD). The temperatures of inlet, oven, and detector were

100°C, 40°C, and 150°C, respectively. The analysis time was 10 min. The amount of permeated gas composition was analyzed by comparing the area under peak with external standard from the calibration curve. The correlation value of accepted calibration curve must be at 99.5% confidence level.



สถาบันวิทยบริการ  
จุฬาลงกรณ์มหาวิทยาลัย

## CHAPTER IV

### RESULTS AND DISCUSSION

#### 4.1 Preparation of $\text{Ce}_{0.5}\text{Zr}_{0.5}\text{O}_2$ mixed oxide

##### 4.1.1 Proper amounts of total solid and solvent for mixed oxide preparation

In 2003, Menad *et al.* [4] prepared a novel  $\text{Ce}_{0.5}\text{Zr}_{0.5}\text{O}_2$  mixed oxide, as a support of Ru catalysts, by the water-in-oil microemulsion method in the dry reforming of methane. It was proved to be a high activity catalytic system with excellent stability under certain reaction condition. However, they reported that in each preparation the mixture of n-heptane and hexanol 1,200 ml was used to obtain 1.45 g of mixed oxide. Obviously, the solvent seems to be too large volume. Therefore, the synthesis of  $\text{Ce}_{0.5}\text{Zr}_{0.5}\text{O}_2$  mixed oxide was attempted using smaller volume of solvent.

The support was prepared by water-in-oil microemulsion method according to Menad *et al.* [4] at 4 different amounts of solid and solvent as shown in Table 4.1. The procedure was shown in Section 3.4.1. After stirring the microemulsion at room temperature for 24 h, it was found that the aggregation was found in entry 4 while the other 3 entries were in emulsion forms. Finally, the mixed oxides from these 3 entries were obtained at approximately equal to the total solid used in each entry. These mixed oxides were further characterized using X-ray diffraction (XRD) and their XRD diagrams were shown in Figure 4.1.

Among these 3 entries, entry 3 had the highest relative intensity. Only the pattern of entry 3 had a good agreement with the XRD library pattern of tetragonal  $\text{Ce}_{0.5}\text{Zr}_{0.5}\text{O}_2$  (JCPDS: 38-1436) with  $2\theta = 28.9, 33.4, 47.8$  although all of them approximately showed the XRD pattern of  $\text{Ce}_{0.5}\text{Zr}_{0.5}\text{O}_2$  mixed oxide.

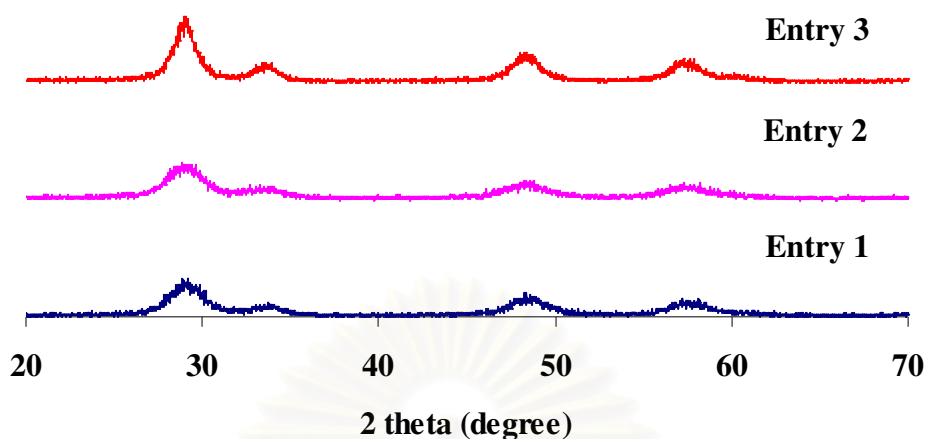


**Figure 4.1** XRD diagrams of  $\text{Ce}_{0.5}\text{Zr}_{0.5}\text{O}_2$  mixed oxide synthesized with different amounts of solid and solvent after calcined in air at  $500^\circ\text{C}$  for 5 h using a ramp of  $4^\circ\text{Cmin}^{-1}$ .

The crystallite size of  $\text{Ce}_{0.5}\text{Zr}_{0.5}\text{O}_2$  mixed oxide was calculated by the Scherrer's equation from half-height width of diffraction peaks. Only the peak at around  $2\theta = 29.0$  could be read by instrument for entries 1 and 2. Therefore, the unit cell parameters of these 2 entries could not be calculated. In addition, these 3 mixed oxides had the approximate crystallite size of 10 nm. Accordingly, the mixed oxide in entry 3 was the most suitable condition for the preparation of tetragonal  $\text{Ce}_{0.5}\text{Zr}_{0.5}\text{O}_2$ .

**Table 4.1** The summarized parameters of  $\text{Ce}_{0.5}\text{Zr}_{0.5}\text{O}_2$  mixed oxide by water-in-oil microemulsion method.

Entry	Solvent (ml)	Weight of total solid (g)	Weight of mixed oxide (g)	Crystallite size (nm)	Unit cell parameter(Å)		
					a	b	c
1	1,330	1.4500	1.4489	9.8	-	-	-
2	250	0.0145	0.0138	10.0	-	-	-
3	250	0.7250	0.7195	10.0	3.73	3.73	5.40
4	250	1.0875	-	-	-	-	-

### 4.1.2 Effect of calcination temperature

In general, the calcination temperature affects on catalyst phase changing. The  $\text{Ce}_{0.5}\text{Zr}_{0.5}\text{O}_2$  mixed oxide was prepared according to Section 4.1.1. After calcination in air at different temperatures for 5 h using a ramp of  $4^\circ\text{C}/\text{min}$ , they were characterized by XRD. The XRD patterns were shown in Figure 4.2.

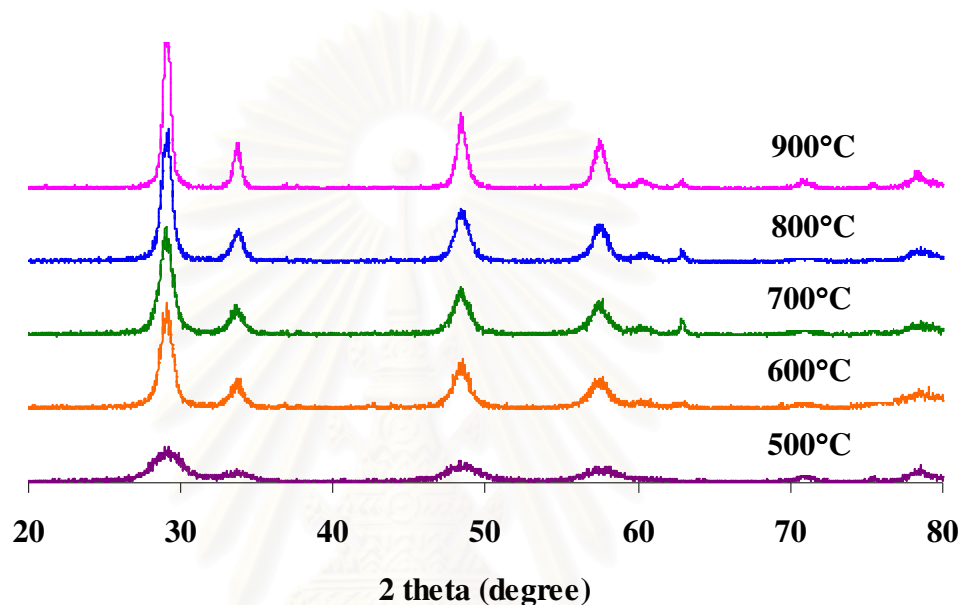


**Figure 4.2** XRD diagrams of  $\text{Ce}_{0.5}\text{Zr}_{0.5}\text{O}_2$  at different calcination temperatures.

The XRD patterns of all mixed oxides, at calcination temperature of 500-800°C, showed the similar reflection corresponding to tetragonal  $\text{Ce}_{0.5}\text{Zr}_{0.5}\text{O}_2$  mixed oxide (JCPDS: 38-1436,  $2\theta = 29.2, 33.7, 48.8$  and  $57.6$ ). When the calcination temperature was increased to 900°C, XRD pattern was shifted to higher  $2\theta$  and not corresponded to tetragonal  $\text{Ce}_{0.5}\text{Zr}_{0.5}\text{O}_2$ . It could be possible that the sintering or phase transfer was emerged.

This result was similar to the report of Sukkaew [20] that the calcination temperature had an effect on prepared support. He found that  $\text{Mg-ZrO}_2$ , prepared by co-precipitation method, was represented the cubic phase at calcination temperature in the range of 600-700°C. When the calcination temperature was increased to 800-950°C,  $\text{ZrO}_2$  monoclinic phase was emerged in concomitant with small amount of

MgO cubic phase. Similar observation of Rezaei *et al.* [21], they found that the increasing calcination temperature from 600 to 800°C led to the tetragonal weight percent decrease and sintering occurred resulting in an increase in crystallite size. It can be concluded that calcination temperature had an important function to catalyst phase changing.

**Table 4.2** Characteristic XRD patterns of tetragonal  $Ce_{0.5}Zr_{0.5}O_2$  mixed oxide at different calcined temperatures.

<b>Calcination temperature (°C)</b>	<b>Crystallite size (nm)</b>
500	10.0
600	11.2
700	10.6
800	11.5
900	-

The data of crystallite size and unit cell parameters were listed in Table 4.2. It was found that a rising of calcination temperature was resulted in an increase of the relative intensity. However, no significant changing of crystallite size was observed at the temperature from 500 to 800°C. It can be concluded from the above data demonstrated that the calcination temperature at 800°C was selected because it gave the highest relative crystallinity with a tiny effect on the crystallite size. Therefore, the preparation of  $Ce_{0.5}Zr_{0.5}O_2$  was used: ratio of solid/solution concentration was that 0.7250 g of solid, 250 ml of solvent and calcination temperature at 800°C.

## 4.2 Effect of $Ce_{1-x}Zr_xO_2$ support containing 15% Ni on dry reforming

### 4.2.1 Preparation and characterization of $Ce_{1-x}Zr_xO_2$ support containing 15% Ni

The nature of the oxide support greatly affects the catalyst due to the aspects of the support structure, metal-support interaction, and acidity-basicity of support. Since  $CO_2$  is well known as an acid gas, adsorption and dissociation of  $CO_2$  could be improved with a basic catalyst. Maraina *et al.* [22] reported that the  $Pt/Al_2O_3$  deactivated very quickly during 20 h on stream at  $800^\circ C$  and a  $CH_4/CO_2$  ratio of 1:1, while the catalysts with  $ZrO_2$  content above 5 %wt. presented improved stability during 60 h. In addition, it was concluded by Ding *et al.* [23] that the effect of the factors on the performance of the catalysts is that support > Ni metal loading >  $MgO$  addition >  $CeO_2$  addition > interaction between metal and support. It has shown the evidence that understanding of the nature and selection of support could be greatly essential for improving the catalyst.

In this section, the  $CeO_2$  promoter was added in order to improve the basicity of support because  $CO_2$  was adsorbed strongly on the surface of basic catalysts. The  $Ce_{1-x}Zr_xO_2$  mixed oxide was prepared by water-in-oil microemulsion followed: the condition in Section 4.1. After impregnated with Ni 15% by weight, the obtained catalysts were calcined in the air at  $800^\circ C$  for 5 h using a ramp of  $4^\circ C/min$ .

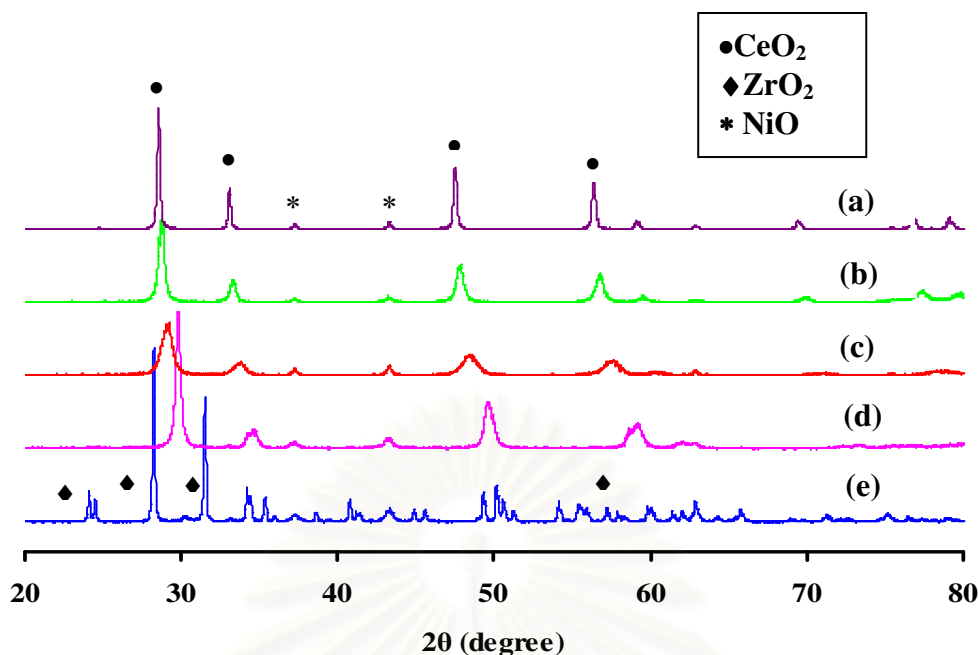


**Figure 4.3** XRD diagrams of  $\text{Ce}_{1-x}\text{Zr}_x\text{O}_2$  support containing 15% Ni: (a) Ni/ $\text{CeO}_2$ , (b) Ni/ $\text{Ce}_{0.75}\text{Zr}_{0.25}\text{O}_2$ , (c) Ni/ $\text{Ce}_{0.5}\text{Zr}_{0.5}\text{O}_2$ , (d) Ni/ $\text{Ce}_{0.15}\text{Zr}_{0.85}\text{O}_2$  and (e) Ni/ $\text{ZrO}_2$ .

Each metal oxide showed its characteristic peak as demonstrated in Figure 4.3. For all catalysts, the hexagonal NiO peaks at around  $2\theta = 37.0$  and  $43.0$  (JCPDS: 89-1701) were very small. In addition, the NiO peaks observed were very broad indicating good dispersion of NiO crystallites in  $\text{Ce}_{0.75}\text{Zr}_{0.25}\text{O}_2$  matrix. The cubic  $\text{CeO}_2$  support containing 15% Ni showed visible peaks at  $2\theta = 28.5$ ,  $33.0$ ,  $47.4$ , and  $56.3$ , which represented the characteristic reflections corresponding to (111), (200), (220), and (311) planes of  $\text{CeO}_2$ , respectively. Whereas the XRD patterns of  $\text{ZrO}_2$  support containing 15% Ni showed characteristic peaks of monoclinic phase ( $2\theta = 24.1$ ,  $24.5$ ,  $28.2$ , and  $31.5$ ). No evidence for extra peaks as regards non-incorporated  $\text{ZrO}_2$  was observed in any XRD patterns of  $\text{Ce}_{1-x}\text{Zr}_x\text{O}_2$  support containing 15% Ni ( $x = 0.25, 0.5, 0.85$ ). These can be suggested that  $\text{ZrO}_2$  could be incorporated into the  $\text{CeO}_2$  lattice to form a solid solution. With regard to the addition of Zr, the diffracting peaks were shifted to higher  $2\theta$  angles. For support containing Ni, the characteristic peaks of the tetragonal  $\text{Ce}_{0.15}\text{Zr}_{0.85}\text{O}_2$  appeared at  $2\theta = 29.7$ ,  $34.6$ ,  $49.6$ , and  $58.6$ . The (101) reflection shifted to  $29.1$  for  $\text{Ce}_{0.5}\text{Zr}_{0.5}\text{O}_2$ . By progressively doping with Ce, the symmetry corresponded increasingly to the cubic for  $\text{Ce}_{0.75}\text{Zr}_{0.25}\text{O}_2$ .



**Table 4.3** Characteristic XRD patterns of  $Ce_{1-x}Zr_xO_2$  support containing 15% Ni.

Peak	Oxide	$2\theta$	d-spacing (nm)	Miller indices	JCPDS
(a)	$CeO_2$	28.5	3.13	(111)	65-2975
		33.0	2.71	(200)	
		47.4	1.91	(220)	
		56.3	1.63	(311)	
(b)	$Ce_{0.75}Zr_{0.25}O_2$	28.7	3.10	(111)	28-0271
		33.4	2.68	(200)	
		47.8	1.90	(024)	
		56.8	1.62	(311)	
(c)	$Ce_{0.5}Zr_{0.5}O_2$	29.1	3.06	(101)	38-1436
		33.8	2.65	(002)	
		48.5	1.87	(112)	
		57.6	1.60	(103)	
(d)	$Ce_{0.15}Zr_{0.85}O_2$	29.7	3.00	(101)	88-2398
		34.6	2.59	(110)	
		49.6	1.84	(112)	
		58.6	1.57	(103)	
(e)	$ZrO_2$	24.1	3.70	(011)	89-1701
		24.5	3.63	(110)	
		28.2	3.16	(-111)	
		31.5	2.83	(111)	

สถาบันวิทยบริการ  
จุฬาลงกรณ์มหาวิทยาลัย

This observation was attributed to the shrinkage of the lattice due to the replacement of  $\text{Ce}^{4+}$  with a smaller cation radius  $\text{Zr}^{4+}$ . For all XRD parameter of  $\text{Ce}_{1-x}\text{Zr}_x\text{O}_2$  support containing 15% Ni was shown in Table 4.3. These results were in good congruent outcome with the results from Xu *et al.* [24]. In agreement with the results by Rodriguez *et al.* [25], the lattice constant decreased with increasing Zr content in Ce-ZrO<sub>2</sub> mixed oxide.

The approximate average sizes  $\text{Ce}_{1-x}\text{Zr}_x\text{O}_2$  were calculated by Scherrer's equation as shown in Table 4.4. It was indicated that the crystallite size slightly decreased while increasing in Zr content.

**Table 4.4** The XRD parameters of  $\text{Ce}_{1-x}\text{Zr}_x\text{O}_2$  support containing 15% Ni.

Oxide	Crystallite size (nm)	Phase	Unit cell parameters (Å)		
			a	b	c
$\text{CeO}_2$	43.3	cubic	5.69	5.69	5.69
$\text{Ce}_{0.75}\text{Zr}_{0.25}\text{O}_2$	20.9	cubic	6.35	6.35	6.35
$\text{Ce}_{0.5}\text{Zr}_{0.5}\text{O}_2$	11.6	tetragonal	3.74	3.74	5.29
$\text{Ce}_{0.15}\text{Zr}_{0.85}\text{O}_2$	10.8	tetragonal	3.66	3.66	5.19
$\text{ZrO}_2$	60.9	monoclinic	5.14	5.19	5.30

Table 4.5 summarized the characteristics of  $\text{Ce}_{1-x}\text{Zr}_x\text{O}_2$  support containing 15% Ni after calcined at 800°C for 5 h. It was found that the BET surface area of  $\text{Ce}_{1-x}\text{Zr}_x\text{O}_2$  support containing 15% Ni ( $x = 0.25, 0.5, 0.85$ ) were much higher than those with the pure  $\text{CeO}_2$  and  $\text{ZrO}_2$ . It could be noticed that the BET surface areas of  $\text{Ce}_{1-x}\text{Zr}_x\text{O}_2$  support containing 15% Ni increased with an arising of Ce content. The results were similar to those of Laosiripojana *et al.* [26]. They prepared Ni/Ce-ZrO<sub>2</sub> samples with the Ce/Zr ratios of 1/0, 1/1, 1/3, and 3/1 by co-precipitation method. They found that the BET surface areas increased with increasing Ce content which obtained around 6.2 to 18.0  $\text{m}^2\text{g}^{-1}$ .

As a general trend, it is observed that ceria induces a slight increase in BET surface area of Ni/Ce-ZrO<sub>2</sub> [5]. However, Rossignol *et al.* [27] found that the surface area of CeO<sub>2</sub>-ZrO<sub>2</sub> mixed oxide was independent of the synthesis method and the CeO<sub>2</sub> concentration.

**Table 4.5** BET surface area and nickel content using XRF of Ce<sub>1-x</sub>Zr<sub>x</sub>O<sub>2</sub> support containing 15% Ni.

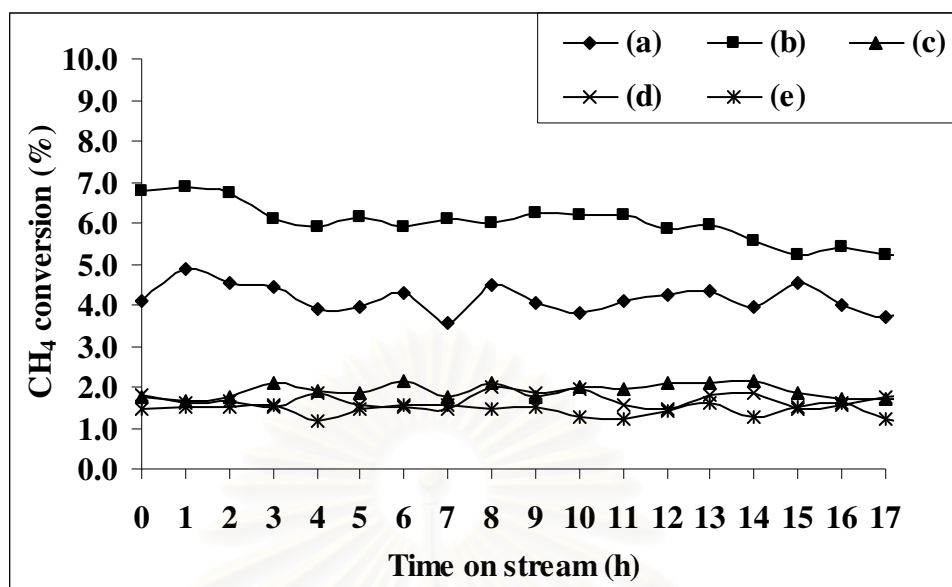
Oxide	Ni % wt (XRF)	Surface area (m <sup>2</sup> g <sup>-1</sup> )	Pore volume (cm <sup>3</sup> g <sup>-1</sup> )	Average pore size(nm)
CeO <sub>2</sub>	13	8	0.13	32.57
Ce <sub>0.75</sub> Zr <sub>0.25</sub> O <sub>2</sub>	13	19	0.20	21.30
Ce <sub>0.5</sub> Zr <sub>0.5</sub> O <sub>2</sub>	14	17	0.18	24.49
Ce <sub>0.5</sub> Zr <sub>0.5</sub> O <sub>2</sub>	0	91	0.18	5.41
Ce <sub>0.15</sub> Zr <sub>0.85</sub> O <sub>2</sub>	13	14	0.13	27.14
ZrO <sub>2</sub>	12	10	0.13	35.12

The average percentage of nickel on Ce<sub>1-x</sub>Zr<sub>x</sub>O<sub>2</sub> support was around 13-14 % by weight obtained by X-ray fluorescence (XRF). These results can be suggested that the rest of nickel was left in the medium along the impregnation. Then, all the prepared Ce<sub>1-x</sub>Zr<sub>x</sub>O<sub>2</sub> support containing 15% Ni was tested in dry reforming of methane.

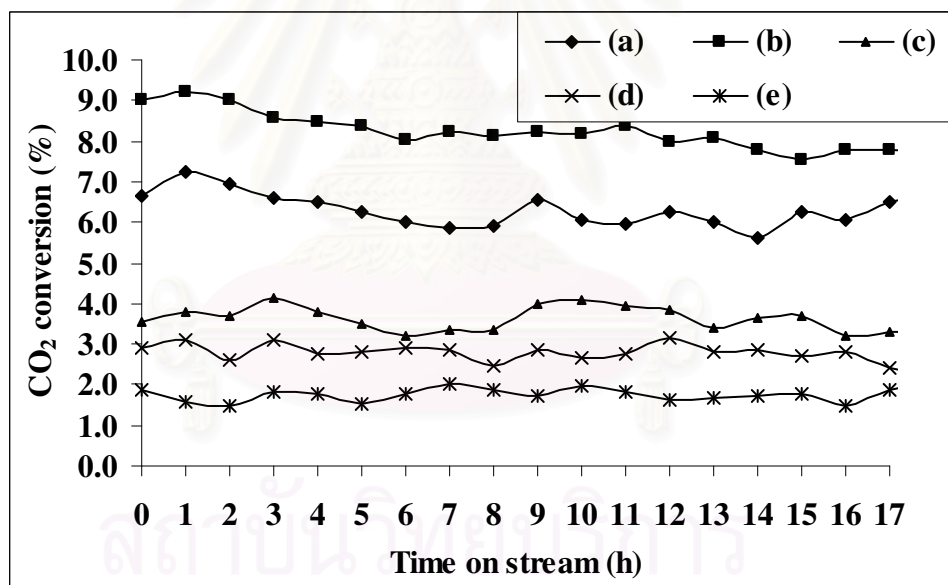
#### 4.2.2 Dry reforming using Ce<sub>1-x</sub>Zr<sub>x</sub>O<sub>2</sub> support containing 15% Ni

In order to select the most suitable catalyst, the dry reforming of methane reaction was carried out over Ce<sub>1-x</sub>Zr<sub>x</sub>O<sub>2</sub> support containing 15% Ni at 450°C. It can be observed that Ni/ZrO<sub>2</sub> was obtained the lowest CH<sub>4</sub> and CO<sub>2</sub> conversion. When ceria was added onto the Ni/ZrO<sub>2</sub> catalyst, CH<sub>4</sub> and CO<sub>2</sub> conversion were significantly increased which was noticeable in Figure 4.4. As a general trend, CH<sub>4</sub> and CO<sub>2</sub> conversions increased according to the CeO<sub>2</sub> content [5]. The conversion of CO<sub>2</sub> was higher than CH<sub>4</sub> conversion because the reverse water-gas shift (RWGS) reaction (equation 2.2) occurs in concomitant with dry reforming of methane.

## Methane conversion



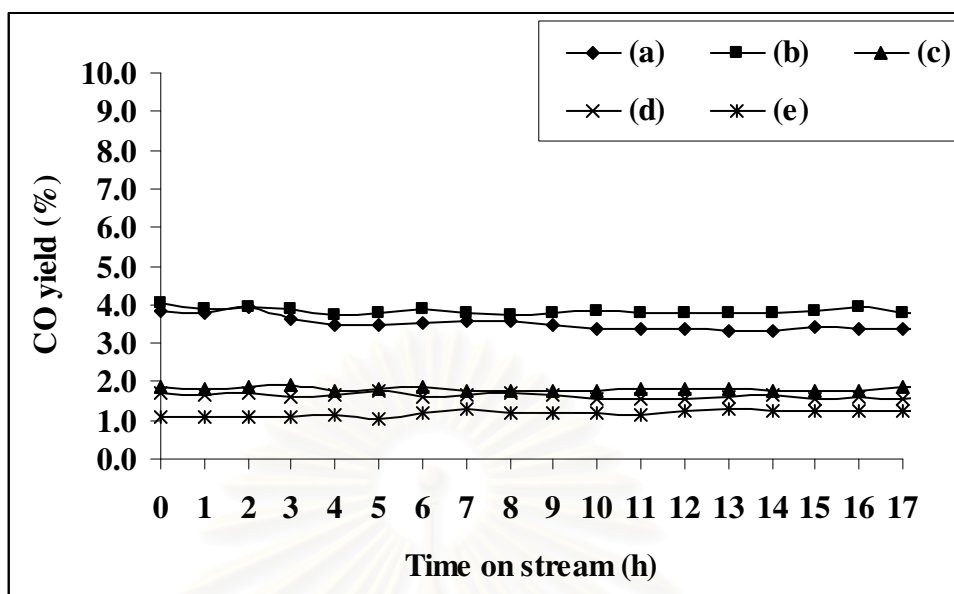
## Carbon dioxide conversion



\*He: carrier gas

**Figure 4.4** CH<sub>4</sub> and CO<sub>2</sub> conversions with time on stream over Ce<sub>1-x</sub>Zr<sub>x</sub>O<sub>2</sub> support containing 15% Ni (reaction condition:  $T = 450^{\circ}\text{C}$ , CH<sub>4</sub>/CO<sub>2</sub> = 1 : 1): (a) Ni/CeO<sub>2</sub>, (b) Ni/Ce<sub>0.75</sub>Zr<sub>0.25</sub>O<sub>2</sub>, (c) Ni/Ce<sub>0.5</sub>Zr<sub>0.5</sub>O<sub>2</sub>, (d) Ni/Ce<sub>0.15</sub>Zr<sub>0.85</sub>O<sub>2</sub> and (e) Ni/ZrO<sub>2</sub>.

## Carbon monoxide yield



\*He: carrier gas

**Figure 4.5** CO yield with time on stream over Ce<sub>1-x</sub>Zr<sub>x</sub>O<sub>2</sub> support containing 15% Ni (reaction condition:  $T = 450^{\circ}\text{C}$ ,  $\text{CH}_4/\text{CO}_2 = 1 : 1$ ): (a) Ni/CeO<sub>2</sub>, (b) Ni/Ce<sub>0.75</sub>Zr<sub>0.25</sub>O<sub>2</sub>, (c) Ni/Ce<sub>0.5</sub>Zr<sub>0.5</sub>O<sub>2</sub>, (d) Ni/Ce<sub>0.15</sub>Zr<sub>0.85</sub>O<sub>2</sub> and (e) Ni/ZrO<sub>2</sub>.

Some differences could be observed. For Ni/Ce<sub>0.5</sub>Zr<sub>0.5</sub>O<sub>2</sub>, Ni/Ce<sub>0.15</sub>Zr<sub>0.85</sub>O<sub>2</sub> and Ni/ZrO<sub>2</sub> catalysts, the conversions attained were much close to each others. It can be proposed that the nature of the catalysts which cerium content was less than or equal 0.5 mole ratio had not much influence on the catalytic behavior of Ni/ZrO<sub>2</sub>. It could be noted that the order of CH<sub>4</sub> conversion was Ni/ZrO<sub>2</sub> < Ni/Ce<sub>0.15</sub>Zr<sub>0.85</sub>O<sub>2</sub> < Ni/Ce<sub>0.5</sub>Zr<sub>0.5</sub>O<sub>2</sub> < Ni/CeO<sub>2</sub> < Ni/Ce<sub>0.75</sub>Zr<sub>0.25</sub>O<sub>2</sub>. In addition, CO yield was increased with increasing Ce content on Ni/Ce<sub>1-x</sub>Zr<sub>x</sub>O<sub>2</sub> catalyst and similar to CH<sub>4</sub> and CO<sub>2</sub> conversions as shown in Figure 4.5. It should also be noted that the carrier gas of the reaction was He which could be overlap with H<sub>2</sub> in GC diagram. Therefore, it could not be detected H<sub>2</sub> peak from the reaction. Likewise, the results by Roh *et al.* [28] showed that the 15% Ni/Ce<sub>0.8</sub>Zr<sub>0.2</sub>O<sub>2</sub> gave more than 97% CH<sub>4</sub> conversion at 800°C.

**Table 4.6** Reaction results over  $\text{Ce}_{1-x}\text{Zr}_x\text{O}_2$  support containing 15% Ni after reaction for 17 h.

Catalyst	Conversion (%)		CO yield (%)	Amount of deposited carbon (%)
	CH <sub>4</sub>	CO <sub>2</sub>		
CeO <sub>2</sub>	4.1	6.3	3.5	10.35
Ce <sub>0.75</sub> Zr <sub>0.25</sub> O <sub>2</sub>	6.1	8.3	3.8	9.36
Ce <sub>0.5</sub> Zr <sub>0.5</sub> O <sub>2</sub>	1.9	3.7	1.8	0.18
Ce <sub>0.15</sub> Zr <sub>0.85</sub> O <sub>2</sub>	1.7	2.9	1.6	1.79
ZrO <sub>2</sub>	1.4	1.7	1.2	0.35

All the catalysts showed a similar slow deactivation along the reaction time. The deactivation of Ni-catalysts during the dry reforming of methane was mainly due to the formation of carbonaceous deposit [5]. The total amount of carbon formation over the Ni/Ce<sub>1-x</sub>Zr<sub>x</sub>O<sub>2</sub> catalysts was obtained from the fact that an increase in the ceria content enhances the carbon formation. The lowest carbon deposition was exhibited by the Ni/ZrO<sub>2</sub> catalyst owing to its low catalytic activity, in accordance with the CH<sub>4</sub> conversion and carbon formation obtained by Montaya *et al.* [5]. Moreover, Ni/CeO<sub>2</sub> catalyst gave the conversion lower than Ni/Ce<sub>0.75</sub>Zr<sub>0.25</sub>O<sub>2</sub> catalyst. Because the redox properties of Ce and the high mobility of lattice oxygen was probably the factors that initially promote catalytic activity in dry reforming of methane, but its easier reducibility under the reaction probably led to decreased CO<sub>2</sub> adsorption on the support surface. In addition, it was reported by Laosiripojana *et al.* [14] that the dry reforming of methane over 8% CeO<sub>2</sub> doped Ni/Al<sub>2</sub>O<sub>3</sub> showed the best activity: 5.0% CH<sub>4</sub> conversion in 400°C and 90% CH<sub>4</sub> conversion in 800°C.

SEM image of Ni/Ce<sub>0.75</sub>Zr<sub>0.25</sub>O<sub>2</sub> catalyst before and used after 17 h reaction showed that there was some carbon on used catalyst surface (Figure 4.6).

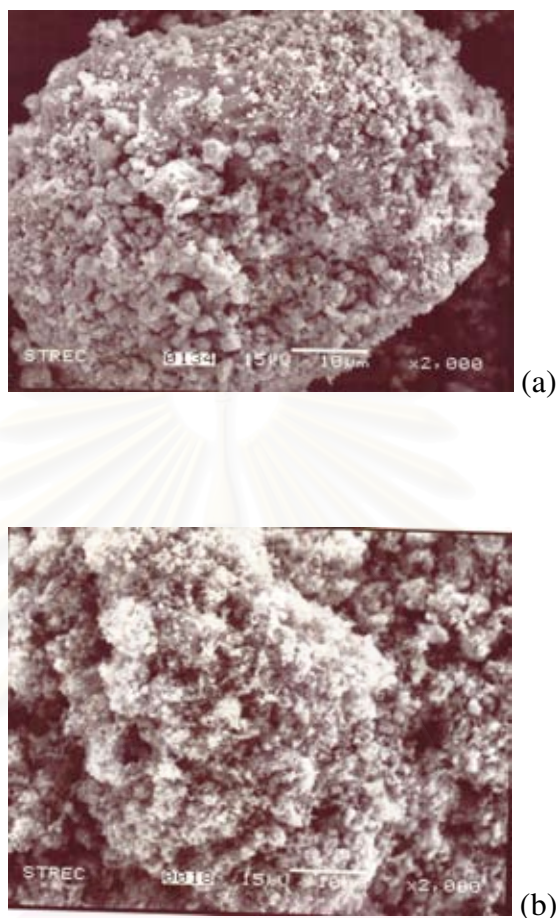


**Figure 4.6** SEM images of Ni/Ce<sub>0.75</sub>Zr<sub>0.25</sub>O<sub>2</sub> catalyst: (a) before the reaction, and (b) after the reaction for 17 h at 450°C.

Within this perspective, the cubic Ce<sub>0.75</sub>Zr<sub>0.25</sub>O<sub>2</sub> containing 15% Ni gave the higher activity than the others. It was recognizable that the cubic Ce-ZrO<sub>2</sub> helps to increase the availability of surface oxygen by a released mechanism during the dry reforming reaction. Moreover, the cubic Ce<sub>0.75</sub>Zr<sub>0.25</sub>O<sub>2</sub> is easily reducible and it contains the better capability of redox couple of Ce<sup>3+</sup> and Ce<sup>4+</sup> than the other phases of Ce-ZrO<sub>2</sub> [11]. Regarding these experiment results, the cubic Ce<sub>0.75</sub>Zr<sub>0.25</sub>O<sub>2</sub> containing 15% Ni was selected for the further investigation.

### 4.3 Effect of Ni content of Ni catalysts on dry reforming

#### 4.3.1 Preparation and characterization of Ni catalysts

The catalytic activity of dry reforming reaction depends on the types of supports, promoters and metals. In addition, metal loading has a direct effect to catalysis activity. The noble metal catalysts generally exhibit promising performance for dry reforming of methane reaction. Although some noble metals show high activity and selectivity for carbon-free operation, high cost and limited availability of noble metals prevent the commercial use of this reaction. Therefore, it is more practical to develop an improved nickel catalyst which exhibits stable operation for a long period of time. The nickel is the best non-noble metallic component as a catalyst for this reaction [25]. In addition, it has shown an excellent activity comparable to noble metal catalysts [2]. Normally, higher loadings are required for nickel catalyst, in which the metal-support interactions are stronger than heavier metals. However, the side reaction caused by nickel is carbon deposition on catalyst which could possibly deposit at the active site of catalyst.

In this section, the study was focused on the investigation of the appropriate amount of nickel loading which gave high conversion of methane and carbon dioxide. The cubic  $\text{Ce}_{0.75}\text{Zr}_{0.25}\text{O}_2$  according to Section 4.2 was used as a support for Ni catalyst. The XRD patterns of the Ni catalysts were shown in Figure 4.7. The amount of nickel loading was varied from 5 to 20% by weight of support and prepared by impregnation. Weak diffraction peaks of the NiO crystalline phase was observed for all Ni catalysts, except the one with 5% nickel (d).



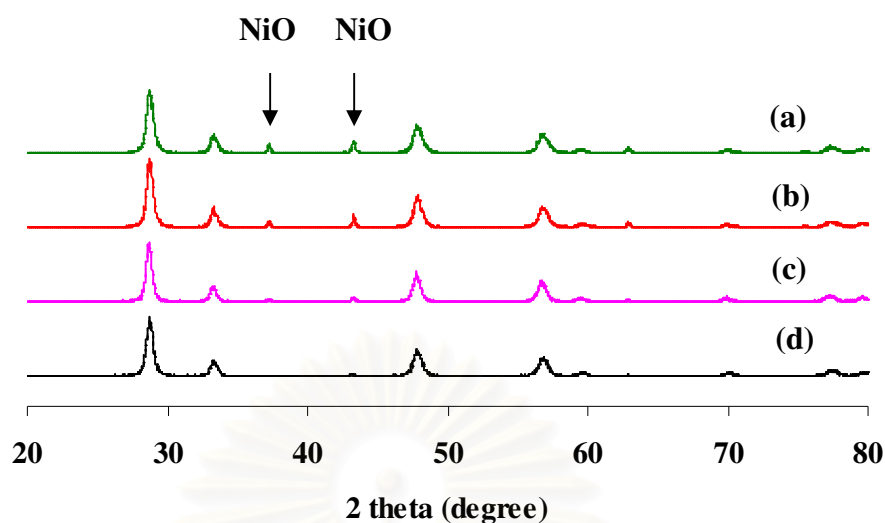


**Figure 4.7** XRD patterns of Ni catalysts at different nickel loading: (a) 20% Ni, (b) 15% Ni, (c) 10% Ni, and (d) 5% Ni.

The intensity of NiO peaks ( $2\theta = 37.2$  and  $43.3$ ) became stronger with an increasing amount of nickel content on the catalyst. It can be suggested that NiO crystallite size was too small to be observed at lower amounts of 5%Ni adding. Therefore, it is possible that part of NiO was existed in the crystalline phase at high nickel content ( $\text{Ni} > 5\% \text{wt}$ ). They were very weak although diffraction peaks of the NiO crystalline phase were observed at 10% NiO. In addition, the crystallinity was increased with increasing the nickel content. Similar observations were reported by Xu *et al* [24]. They found that the NiO particle size was too small to be observed at lower amount of NiO ( $\text{Ce}_{1-x}\text{Ni}_x\text{O}_2$ ,  $x = 0.1$ ). Although diffraction peaks of the NiO crystal phase were observed when  $x = 0.5$ , they were still very weak when compared with the mixture of  $\text{CeO}_2$  and NiO ( $\text{CeO}_2:\text{NiO} = 0.5:0.5$ ). Additionally, the results were shown that the  $\text{Ce}_{0.75}\text{Zr}_{0.25}\text{O}_2$  had cubic phase for all Ni catalysts as illustrated by the XRD patterns which were corresponding to (111), (200), (024), (220), and (311) planes (JCPDS: 28-0271).

It can be observed that the relative intensity of NiO increased with increasing nickel loading. According to broad peaks of 5% Ni, it was unable to detect the NiO. When more nickel was loaded, the relative intensity was higher. Due to the fact that it could be generated the process of the metal sintering on the support surface at higher nickel loading ( $\text{Ni} > 5\%$ ).

To study on Ni catalyst property, the BET surface area of the catalysts was observed after the reduction treatment. The 20%Ni catalyst showed the decreasing in both the surface area and pore volume. It can be assumed that some Ni was deposited in the rest of catalyst pore or metal sintering. However, 15%Ni catalyst gave the highest surface area. Possibly, NiO deposited around the pore. All catalysts gave approximately average pore size of 24.4 nm and similar surface area: impregnation of Ni on supports did not disturb the support structure. The BET parameter of Ni catalyst was shown in Table 4.7. In addition, this result was related to the work of Roh *et al.* [28]. They reported that Ni/Ce<sub>0.8</sub>Zr<sub>0.2</sub>O<sub>2</sub> synthesized by co-precipitation/digestion method shows intensifying NiO peaks become stronger with increase in Ni content. It is expected that well Ni dispersion could be obtained with 15% Ni loading.

**Table 4.7** BET surface area of Ni catalysts.

Catalyst	Surface area ( $\text{m}^2\text{g}^{-1}$ )	Pore volume ( $\text{cm}^3\text{g}^{-1}$ )	Average pore size (nm)
5%Ni-Ce <sub>0.75</sub> Zr <sub>0.25</sub> O <sub>2</sub>	15	0.12	24.4
10%Ni-Ce <sub>0.75</sub> Zr <sub>0.25</sub> O <sub>2</sub>	16	0.18	21.3
15%Ni-Ce <sub>0.75</sub> Zr <sub>0.25</sub> O <sub>2</sub>	20	0.20	24.4
20%Ni-Ce <sub>0.75</sub> Zr <sub>0.25</sub> O <sub>2</sub>	17	0.16	24.4

The impregnated Ni on Ce<sub>0.75</sub>Zr<sub>0.25</sub>O<sub>2</sub> was determined by XRF and EDX. As the results shown in Table 4.8, the nickel content from XRF was similar to EDX for all catalysts. However, those from EDX were much higher than XRF. It could be due to some inhomogeneous nickel dispersion.

**Table 4.8** The amount of nickel content deposited on Ce<sub>0.75</sub>Zr<sub>0.25</sub>O<sub>2</sub> using XRF and EDX.

Nickel content (% wt)	Deposited nickel (% wt)	
	XRF	EDX
5	3	4
10	8	9
15	12	13
20	17	17

The dispersion of nickel on the support was obtained by EDX mapping as shown in Figure 4.8. As a result of such figure, it can be interpreted that all supports obtained well dispersion of nickel. The increasing of mapping area was obtained when increased the nickel content. However, the pictures were not definitely clear as regards some charging because it was either non-conductivity or surface roughness.

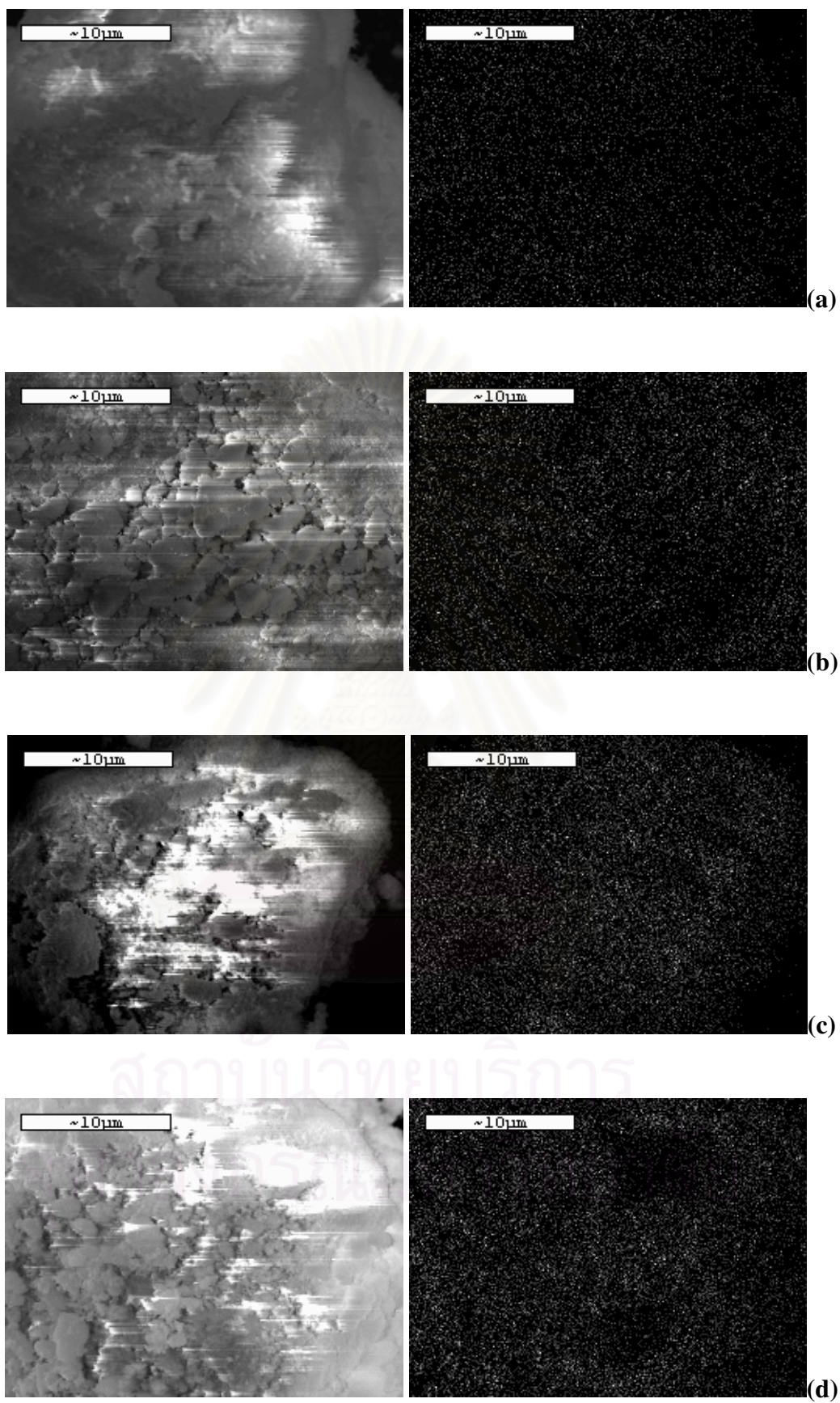


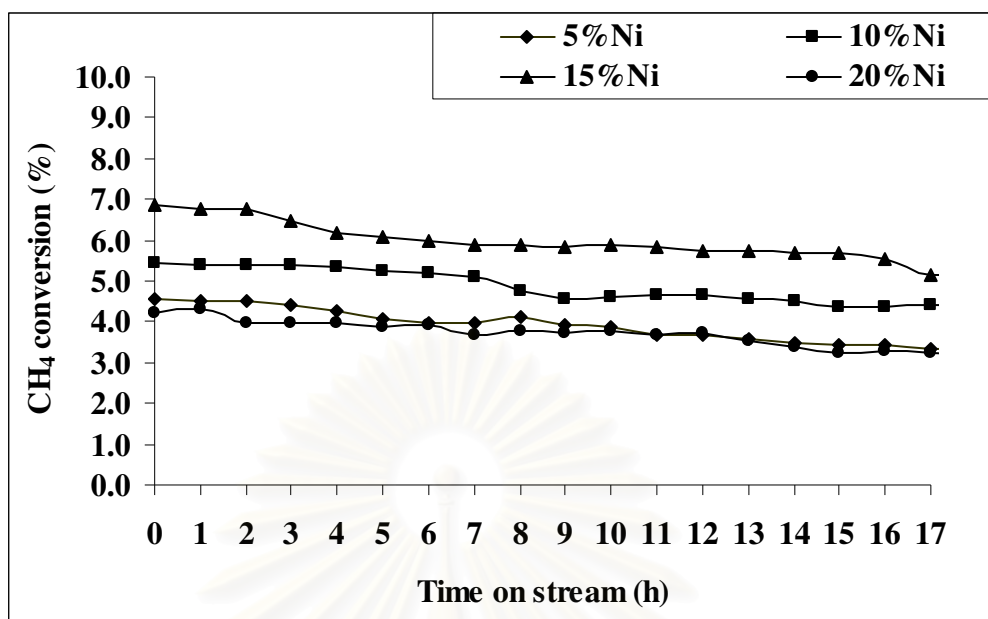
**Figure 4.8** EDX mapping of Ni catalysts: (a) 5% Ni, (b) 10% Ni, (c) 15% Ni, and (d) 20% Ni.

### 4.3.2 Dry reforming using Ni catalysts

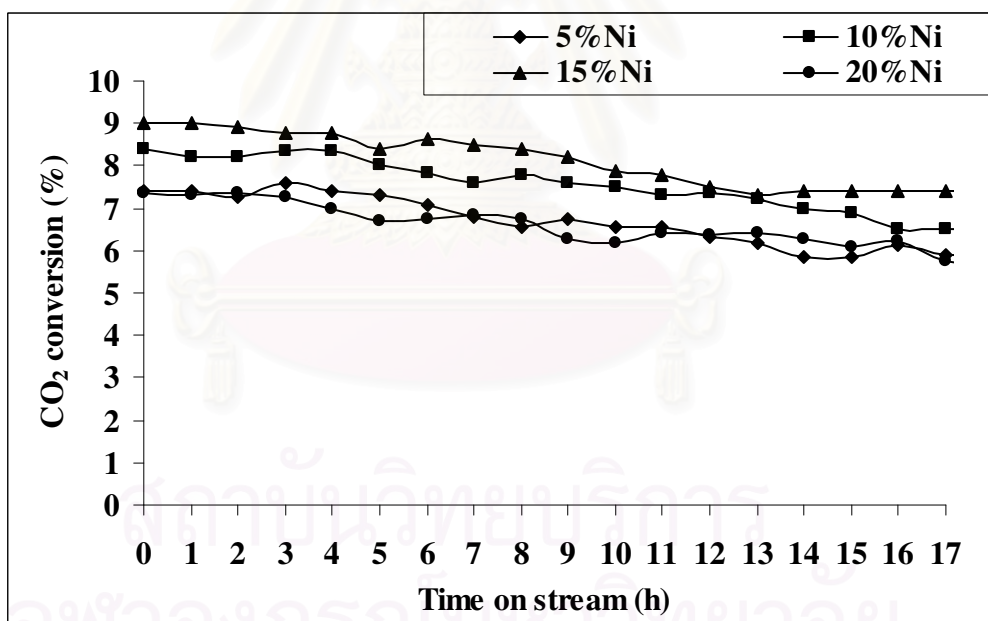
In this part, the amount of nickel on the support was considered in order to give the suitable catalyst. Catalytic activity with regard to the conversion of methane and carbon dioxide were measured at atmospheric pressure for 17h over a series of Ni catalysts with the nickel content of 5-20 % by weight (Figure 4.9). It was observed that the 5%Ni catalyst gave the lowest both of CH<sub>4</sub> and CO<sub>2</sub> conversions. In addition, the conversions increased with increasing the nickel content except in 20%Ni catalyst. These results were similar trend to CO yield (Figure 4.10).

Table 4.9 showed the average percent conversion and the amount of deposited carbon. Among the catalysts, 15%Ni catalyst exhibited the highest activity even though a large amount of carbon was deposited on catalyst surface during the reaction. It is possible to elaborate that it might be attributed to the participation of carbon species as a reaction intermediate in the dry reforming of methane. In addition, it can be suggested that the decreasing in metal dispersion could obtained in 20%Ni catalyst which led to lower conversions obtained [15]. In all cases, CO<sub>2</sub> conversion was higher than CH<sub>4</sub> conversion as a result of contribution of reverse water gas shift (RWGS) reaction. It is likely that the activity and stability of 15%Ni catalyst was corresponded to the BET surface area as shown in Table 4.8. Similar to previous report, 13% Ni/ZrO<sub>2</sub> catalyst gave the highest for dry reforming of methane among the nickel content between 2.5 and 23 % at 750°C. Even though, a large amount of carbon was deposited on catalyst surface during the reaction (reaction conditions:  $T = 750^{\circ}\text{C}$ , CH<sub>4</sub>:CO<sub>2</sub>:N<sub>2</sub> = 1:1:3,  $P = 1 \text{ atm}$ ) [9].

## Methane conversion



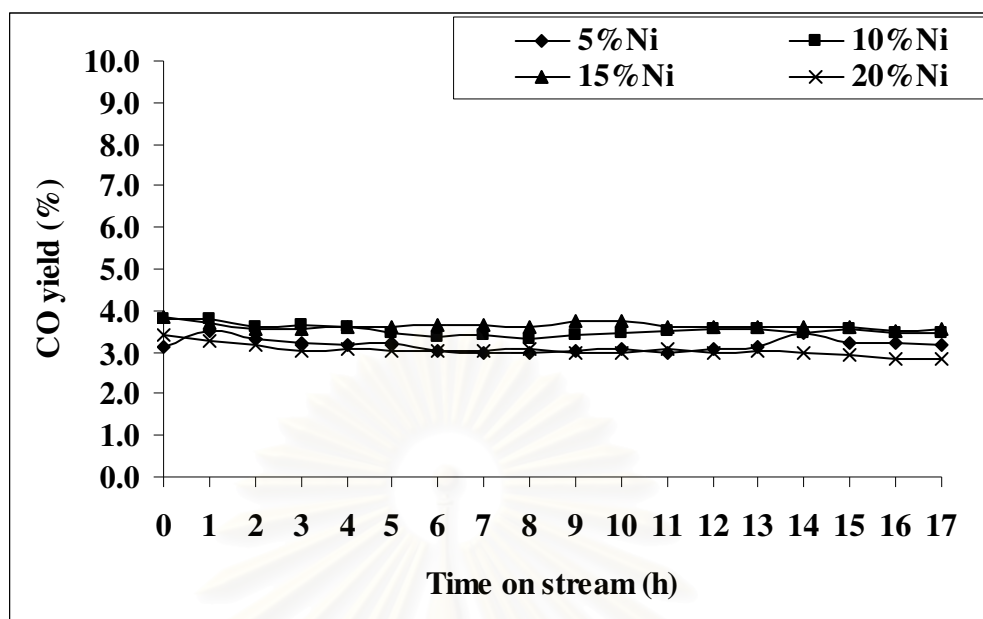
## Carbon dioxide conversion



\*He: carrier gas

**Figure 4.9** CH<sub>4</sub> and CO<sub>2</sub> conversions with time on steam over Ni catalysts in dry reforming of methane (reaction condition:  $T = 450^{\circ}\text{C}$ , CH<sub>4</sub>/CO<sub>2</sub> = 1 : 1).

## Carbon monoxide yield



\*He: carrier gas

**Figure 4.10** CO yield with time on stream over Ni catalysts in dry reforming of methane (reaction condition:  $T = 450^{\circ}\text{C}$ ,  $\text{CH}_4/\text{CO}_2 = 1 : 1$ ).

This result was also similar to previous report discussing the effect of Ni loading on the co-precipitated Ni/Ce<sub>0.8</sub>Zr<sub>0.2</sub>O<sub>2</sub> catalysts. It was found that 15%Ni co-precipitated with Ce<sub>0.8</sub>Zr<sub>0.2</sub>O<sub>2</sub> having cubic phase gave synthesis gas with CH<sub>4</sub> conversion more than 97% at 800°C and such activity was maintained without significant loss during the reaction for 100 h. Moreover, both CH<sub>4</sub> and CO<sub>2</sub> conversion increased with the rise of Ni loading up to 15%, and then they decreased (reaction conditions:  $T = 800^{\circ}\text{C}$ ,  $\text{CH}_4:\text{CO}_2:\text{N}_2 = 0.98:1.02:1.00$ ,  $P = 1 \text{ atm}$ ) [28].

The amount of deposited carbon was increased with increasing of nickel content. In addition, 20%Ni was obtained the conversions lower than 15%Ni while carbon deposition was higher. This may be because of the fact that the 20% Ni catalyst has relative low Ni dispersion and large Ni particle size from metal sintering. Therefore, it was obtained in low coke resistance during the reaction.

**Table 4.9** Reaction results over Ni catalysts after reaction for 17 h.

Catalyst	Conversion (%)		CO yield (%)	Amount of deposited carbon (%)
	CH <sub>4</sub>	CO <sub>2</sub>		
5%Ni-Ce <sub>0.75</sub> Zr <sub>0.25</sub> O <sub>2</sub>	3.9	6.5	3.4	4.54
10%Ni-Ce <sub>0.75</sub> Zr <sub>0.25</sub> O <sub>2</sub>	5.0	7.6	3.7	4.67
15%Ni-Ce <sub>0.75</sub> Zr <sub>0.25</sub> O <sub>2</sub>	5.8	8.3	3.8	10.51
20%Ni-Ce <sub>0.75</sub> Zr <sub>0.25</sub> O <sub>2</sub>	3.8	6.3	3.2	12.43

Therefore, the amount of nickel loading had an effect on catalysis activity. It was reported by Yan *et al.* [10] that they prepared Al<sub>2</sub>O<sub>3</sub> support by the incipient wetness impregnation method. They found that conversion of CH<sub>4</sub> and CO<sub>2</sub> gradually increased with elevated Ni metal loading, reaching a maximum level at 8 wt%. (Reaction condition reaction:  $T = 727^{\circ}\text{C}$ , CH<sub>4</sub>:CO<sub>2</sub> = 1:1,  $P = 1$  atm). From the above results, 15%Ni catalyst was selected for further investigation in order to find the optimum catalyst for dry reforming of methane at 450°C.

#### 4.4 Effect of Ru content of Ni-Ru bimetallic catalysts on dry reforming

##### 4.4.1 Preparation and characterization of Ni-Ru bimetallic catalysts

To improve the catalyst activity, the addition of ruthenium into nickel catalyst was attempted. It has been reported that bimetallic catalysts exhibited superior activity, selectivity and deactivation resistance to monometallic catalyst [19]. Crisafulli *et al.* [29] reported that the addition of Ru or Pd onto Ni/SiO<sub>2</sub> had a strong influence on the catalytic performance towards the dry reforming of methane. In addition, low loadings (about 1% ~ 5%) of the noble metals are usually sufficient due to their effective performance [30]. On this basis, the effect of Ru content on the activity of Ni catalyst towards the dry reforming of methane was studied.



The various amount of Ru was added onto the optimum Ni catalyst from Section 4.3. They were characterized by XRD. Figure 4.11 showed the XRD patterns of these catalysts. All supports gave the characteristic peaks at around  $2\theta = 28.0, 33.0, 47.0,$  and  $56.0$  which corresponding to (111), (200), (024), and (220) planes (JCPDS: 28-0271). These data thus indicated that all of them had cubic structure of  $\text{Ce}_{0.75}\text{Zr}_{0.25}\text{O}_2$ .

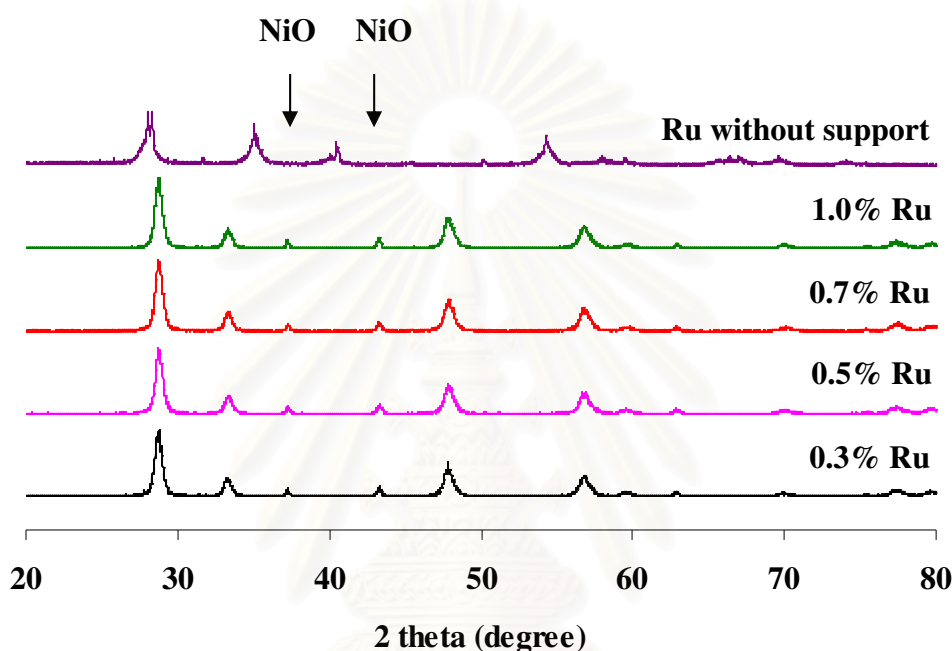


**Figure 4.11** XRD patterns of Ni-Ru catalyst with various ruthenium loadings.

The appearance of the peaks at around  $2\theta = 37.0$  and  $43.0$  indicated the presence of hexagonal NiO (JCPDS: 78-0643). Unfortunately, no peaks corresponding to Ru could be observed. These could be due to the tiny amount of Ru deposited on the support which could not be detected by XRD. Table 4.10 showed the XRD parameter of NiO. Among these catalysts, 0.7%Ru catalyst was the highest ruthenium loading which the crystallite size of NiO was unchanged. It can be suggested that 0.3 to 0.7%Ru loading obtained the good quality of dispersion of NiO as a broad peak [5]. Moreover, when the amount of Ru reached to 1.0%, the crystallite size of NiO was greatly increased to 45 nm.

**Table 4.10** The crystallite size of NiO on Ni-Ru bimetallic catalysts.

<b>Ru content(% wt)</b>	<b>Crystallite size of NiO (nm)</b>
0.3	38
0.5	39
0.7	39
1.0	45

Table 4.11 showed the surface area of Ni-Ru bimetallic catalysts obtained by BET. The surface area increased with increasing ruthenium content from 0.3 to 0.7 %Ru. Beyond 0.7% Ru loading, it seemed that surface area was not affected. It seems that excessive ruthenium caused the metal sintering. These results were conformed to the XRD patterns that the crystallite size of NiO was suddenly raised up when the impregnated ruthenium was 1.0 %Ru.

**Table 4.11** The BET surface area of Ni-Ru bimetallic catalysts.

<b>Ru content (% wt)</b>	<b>Surface area (m<sup>2</sup>g<sup>-1</sup>)</b>	<b>Pore volume (cm<sup>3</sup>g<sup>-1</sup>)</b>	<b>Average pore size (nm)</b>
0.3	14	0.16	32.57
0.5	18	0.20	37.87
0.7	19	0.24	34.14
1.0	19	0.22	32.57

The percentage of metal content was obtained by XRF. As shown in Table 4.12, the nickel content in all catalysts was approximately around 13%. However, the nickel content from XRF was less than the nickel loading, it can be stated that the rest of metal was left in the medium used during the impregnation. These results were similar to those using ruthenium content.

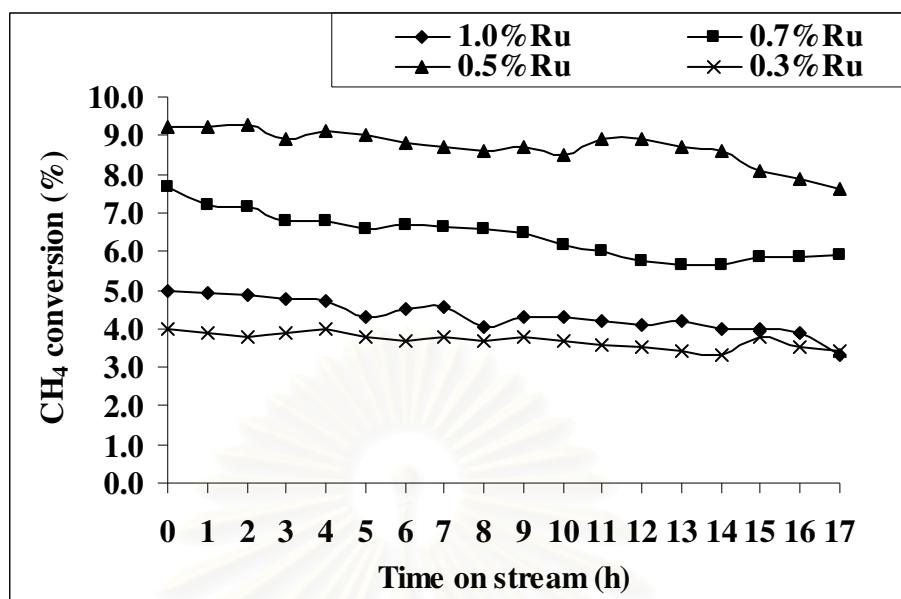
**Table 4.12** Ruthenium and nickel content of catalysts determined by XRF.

<b>Ru loading (% wt)</b>	<b>Ru (% wt)</b>	<b>Ni (% wt)</b>
0.3	0.27	13
0.5	0.42	13
0.7	0.68	14
1.0	0.89	13

#### 4.4.2 Dry reforming using Ni-Ru bimetallic catalysts

In this section, the Ni-Ru bimetallic catalysts supported on  $\text{Ce}_{0.75}\text{Zr}_{0.25}\text{O}_2$  according to Section 4.4.1 were tested in dry reforming of methane which comparing to Ni catalyst supported on  $\text{Ce}_{0.75}\text{Zr}_{0.25}\text{O}_2$  and Ru catalyst supported on  $\text{Ce}_{0.75}\text{Zr}_{0.25}\text{O}_2$ . The experimental condition was used according to Section 3.4.4 with used argon as a carrier gas. Therefore, it can be observed the  $\text{H}_2$  gas from the reaction. The results of dry reforming activity were shown in Figure 4.12. The conversion of  $\text{CH}_4$  was higher than  $\text{CO}_2$  for all catalysts because of the reverse water gas shift reaction. For Ni-Ru bimetallic catalyst, the increasing of Ru content led to increase the catalytic activity. The catalytic performance of Ni-Ru bimetallic catalysts were strongly dependent the Ru content. It was possible to observe that growing amounts of Ru continuously improved both activity and stability. However, 1%Ru on Ni catalyst was obtained the lowest conversion among Ni-Ru bimetallic catalyst. It can be suggested that metal sintering or low surface area caused decreasing in catalytic activity. According to the suggestion of published paper about bimetallic catalysts [19], the formation of Ni-Ru clusters on silica caused an obvious improvement in the activity and stability of the bimetallic system due to an increase in the metallic dispersion of Ni. Moreover, they were suggested that the Ni-Ru particles had a surface mainly covered by nickel, in accordance with the previous results reported on the same bimetallic system [31].

## Methane Conversion



## Carbon dioxide conversion

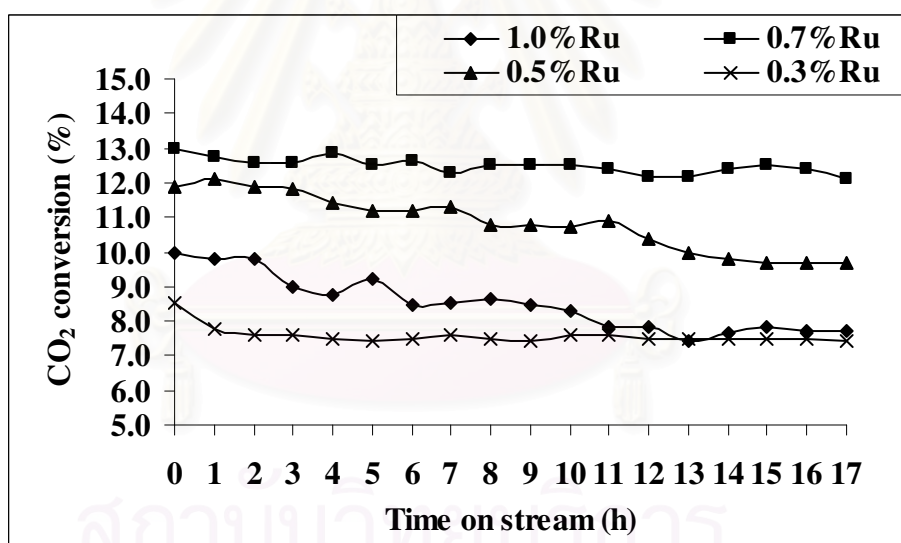
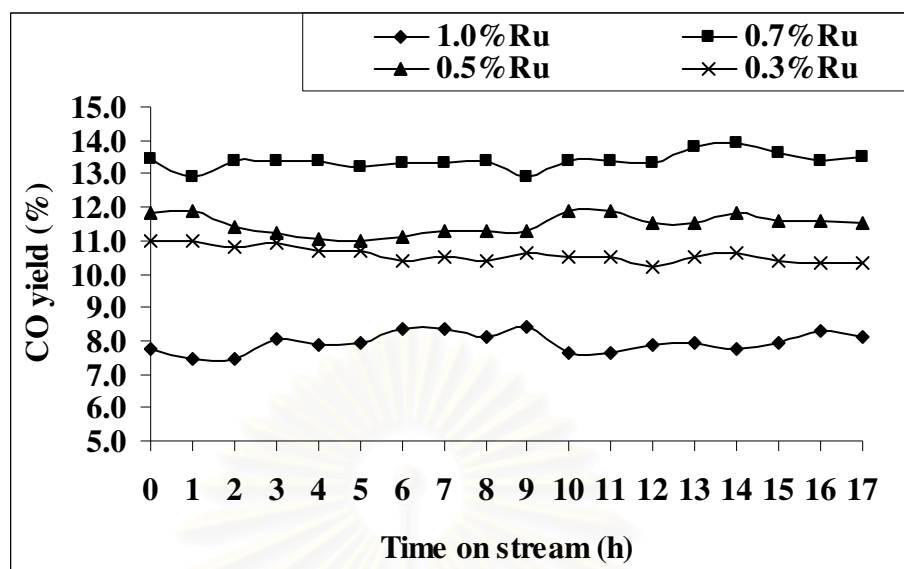


**Figure 4.12** CH<sub>4</sub> and CO<sub>2</sub> conversions with time on steam over Ru on Ni catalysts in dry reforming of methane (reaction condition:  $T = 450^{\circ}\text{C}$ , CH<sub>4</sub>/CO<sub>2</sub> = 1 : 1).

## Carbon monoxide yield



## Hydrogen yield

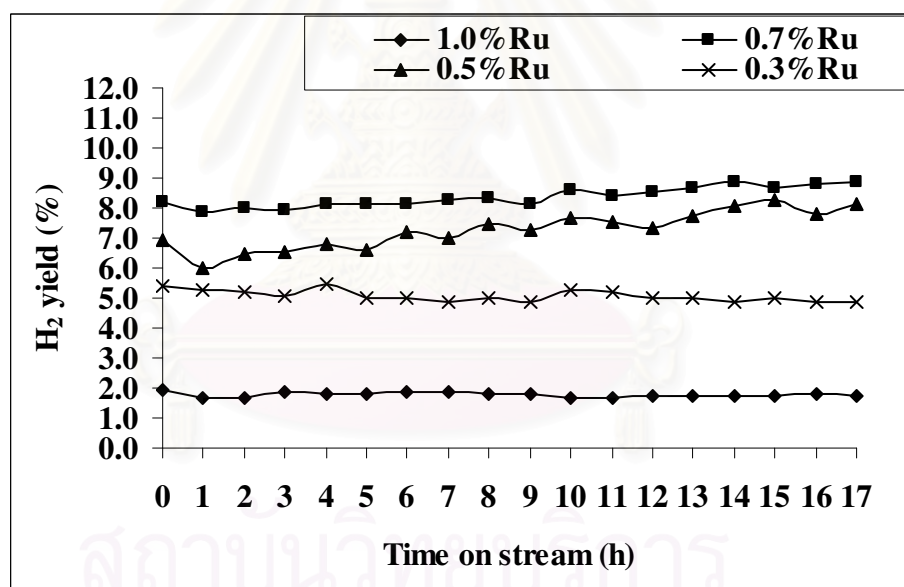


**Figure 4.13** CO and H<sub>2</sub> yields with time on stream over Ru on Ni catalysts in dry reforming of methane (reaction condition:  $T = 450^{\circ}\text{C}$ ,  $\text{CH}_4/\text{CO}_2 = 1 : 1$ ).

By comparing to monometallic catalyst, 0.7%Ru on Ni catalyst gave higher methane conversion than 15%Ni/Ce<sub>0.75</sub>Zr<sub>0.25</sub>O<sub>2</sub> and 1%Ru/Ce<sub>0.75</sub>Zr<sub>0.25</sub>O<sub>2</sub>. It should be noted that the deactivation of 15%Ni/Ce<sub>0.75</sub>Zr<sub>0.25</sub>O<sub>2</sub> was obtained at high conversion. These results had similar trend to CO and H<sub>2</sub> yield as shown in Figure 4.13. Moreover, the obtained H<sub>2</sub> was less than CO which confirmed the reverse water gas shift reaction. The amount of deposited carbon was suppressed by addition of Ru as shown in Table 4.13. However, some of carbon deposition was obtained according to CH<sub>4</sub> conversion.

**Table 4.13** Reaction results over Ru-Ni bimetallic catalysts.

Ni (%)	Ru (%)	Conversion (%)		Yield (%)		Amount of deposited carbon (%)
		CH <sub>4</sub>	CO <sub>2</sub>	CO	H <sub>2</sub>	
15	0	5.8	8.3	3.8	4.1	10.51
15	0.3	3.7	7.7	10.7	5.2	10.31
15	0.5	8.6	10.7	11.7	7.3	9.20
15	0.7	6.9	11.8	13.4	8.4	6.50
15	1.0	4.2	8.4	7.9	1.8	1.57
0	1	1.6	3.1	1.6	N/A	0.30

Considering the report [32] that carbon whiskers have high mechanical strength and the catalyst particle was destroyed when the whiskers hit the pore walls, the build-up of whisker carbon on a catalyst should be suppressed. Since it was reported [33] that the rate of carbon formation on noble metals was far less than on nickel. Thus, a few atomic layers of carbon were observed on the most of the Ru catalyst surface. Crisafulli *et al.* [29] suggested the formation of more reactive carbonaceous species on Ru-Ni/SiO<sub>2</sub> catalyst was less than on Ni/SiO<sub>2</sub> catalyst during the dry reforming of methane, considering the results of the temperature-programmed surface reaction of the deposited carbonaceous species with H<sub>2</sub> (H<sub>2</sub>-TPSR) after a CH<sub>4</sub>-decomposition experiment.

From the results, the 15%Ni-0.7%Ru/Ce<sub>0.75</sub>Zr<sub>0.25</sub>O<sub>2</sub> bimetallic catalyst gave the highest catalytic activity and stability in dry reforming of methane at 450°C than monometallic catalyst for 17 h. Owing to the fact that there is a price difference between noble metals and Ni, promotion of Ni by a small amount of Ru is more practical to industrial application.



สถาบันวิทยบริการ  
จุฬาลงกรณ์มหาวิทยาลัย

## CHAPTER V

### CONCLUSIONS AND SUGGESTIONS

The results presented in this research demonstrated that the cubic  $\text{Ce}_{0.75}\text{Zr}_{0.15}\text{O}_2$  containing 15% Ni had an advantage for dry reforming of methane. During the reaction, the gas-solid reaction on  $\text{Ce}_{0.75}\text{Zr}_{0.15}\text{O}_2$  surface took place simultaneously with the side reactions on the surface of Ni, which was the reverse water gas shift reaction. These side reactions led to deposit of carbon on catalyst surface and decreased the catalytic activity. However, it should also be noted that pure ceria resulted in the oxidation of Ni. It reduced the reforming activity. Therefore, the cubic  $\text{Ce}_{0.75}\text{Zr}_{0.15}\text{O}_2$  support provided more stable catalysts than  $\text{CeO}_2$  or  $\text{ZrO}_2$  containing 15% Ni because  $\text{ZrO}_2$  stabilized the cubic structure and enhanced oxygen storage capacity.

From the results of Ni loading from 5 to 20 %, it showed that  $\text{CH}_4$  and  $\text{CO}_2$  conversions in the reactions increased with increasing nickel content up to 15% and then decreasing at 20%. It can be suggested that the metal dispersion on the support surface was decreased after 15% of nickel loading. In addition, the sintering of nickel oxide was obtained according to the increasing of NiO crystallite size. A small amount of Ru doped over 15% Ni catalyst proved to be effective in  $\text{CH}_4$  and  $\text{CO}_2$  conversions. It is noteworthy that the carbon formation on Ni catalyst was greatly suppressed by doping a small amount of Ru onto the catalyst. Moreover, it was proved that the bimetallic catalyst had better catalytic activity than monometallic catalyst.

Due to the above mentioned, the 0.7%Ru-15%Ni/ $\text{Ce}_{0.75}\text{Zr}_{0.15}\text{O}_2$  bimetallic catalyst exhibited the highest activity in the dry reforming reaction at 450°C for 17 h.



**Suggestion**

- According to previous report [8], they studied in dry reforming of methane at 400 to 900°C to obtain the highest CH<sub>4</sub> and CO<sub>2</sub> conversions. They found that the best activity over 8% CeO<sub>2</sub> doped Ni/Al<sub>2</sub>O<sub>3</sub> was obtained at 900°C. Therefore, catalytic activity of Ni-Ru bimetallic catalyst supported on Ce<sub>0.75</sub>Zr<sub>0.25</sub>O<sub>2</sub> shall be investigated in dry reforming of methane at the temperature range of 500 - 900°C.

- It will be interesting to study the performance of Ni-Ru bimetallic catalyst supported on Ce<sub>0.75</sub>Zr<sub>0.25</sub>O<sub>2</sub> in dry reforming of methane in palladium membrane reactor comparing to the conventional reactor. It is expected that higher conversion from palladium membrane reactor will be resulted since H<sub>2</sub> produced from reaction can be simultaneously separated via the diffusion through palladium membrane.



สถาบันวิทยบริการ  
จุฬาลงกรณ์มหาวิทยาลัย

## REFERENCES

- [1] Ronggang, D.; Zifeng, Y.; Linhua, S.; Xinmei L., A review of dry reforming of methane over various catalysts, *Journal of Natural Gas Chemistry*, **2001**, 3, 237-254.
- [2] Zhaoyin, H.; Ping, C.; Heliang, F.; Xiaoming, Z.; Tatsuaki, Y., Production of synthesis gas via methane reforming with CO<sub>2</sub> on noble metals and small amount of noble-(Rh-) promoted Ni catalysts, *International Journal of Hydrogen Energy*, **2006**, 31, 555-561.
- [3] Carmelo, C.; Salvatore, S.; Simona, M.; Luigi, S., Ni-Ru bimetallic catalysts for the CO<sub>2</sub> reforming of methane, *Applied Catalysis A: General*, **2002**, 225, 1-9.
- [4] Menad, S.; Ferreira-Aparicio, P.; Cherift, O.; Guerrero-Ruiz, A.; Rodriguez-Ranos, I., Designing new high oxygen mobility supports to improve the stability of Ru catalysts under dry reforming of methane, *Catalysis Letters*, **2003**, 89, 63-67.
- [5] Montoya, J.A.; Romero-Pascual, E.; Gimón, C.; Del Angel, P.; Monzon, A., Methane reforming with CO<sub>2</sub> over Ni/ZrO<sub>2</sub>-CeO<sub>2</sub> catalysts prepared by sol-gel, *Catalysis Today*, **2000**, 63, 71-85.
- [6] Takayasu, O.; Matsuura, I., *Proceeding of 10<sup>th</sup> ICC*, Budapest, 1992:1951.
- [7] Hall, R.B.; Castro, M.; Kim, C.M.; Mims, C.A., *Proceeding of 10<sup>th</sup> ICC*, Elsevier Science, Baltimore, July, 1996, USA.
- [8] Erdohelyi, A.; Cserenyi, J.; Solymosi, F., Activation of CH<sub>4</sub> and its reaction with CO<sub>2</sub> over supported Rh catalysts, *Journal of Catalysis*, **1993**, 141, 287-289.
- [9] Zhang, Z.L.; Verykoi, X.E., Carbon dioxide reforming of methane to synthesis gas over supported Ni catalysts, *Catalysis Today*, **1994**, 21, 589-595.
- [10] Yan, Z.F.; Ding, R.G.; Song, L.H.; Qian, L., Mechanistic study of carbon dioxide reforming with methane over supported nickel catalyst, *Energy and Fuels*, **1998**, 12(6), 1114-1120.
- [11] Hyun-Seog, R.; Potdar, H. S.; Ki-Won, J., Carbon dioxide reforming of methane over co-precipitated Ni-CeO<sub>2</sub>, Ni-ZrO<sub>2</sub> and Ni-Ce-ZrO<sub>2</sub> catalysts, *Catalysis Today*, **2004**, 93-95, 39-44.

- [12] Kuznetsova, T.G.; Sadykov, V.A.; Veniaminov, S.A.; Alikina, G.M.; Moroz, E.M.; Rogov, V.A.; Martyanov, O.N.; Yudanov, V.F.; Abornev, I.S.; Neophytides, S., Methane transformation into syngas over Ce-Zr-O system: role of the surface/bulk promoters and oxygen mobility, *Catalysis Today*, **2004**, 91-92, 161-164.
- [13] Xiancai, L.; Min, W.; Zhihua, L.; Fei, H., Studies on nickel-based catalysts for carbon dioxide reforming of methane, *Applied Catalysis A: General*, **2005**, 290, 81-86.
- [14] Laosiripojana, N.; Sutthisripok, W.; Assabumrungrat, S., Synthesis gas production from dry reforming of methane over CeO<sub>2</sub> doped Ni/Al<sub>2</sub>O<sub>3</sub>: Influence of the doping ceria on the resistance toward carbon formation, *Chemical Engineering Journal*, **2005**, 112, 13-22.
- [15] Wen-Sheng, D.; Hyun-Seog, R.; Ki-Won, J.; Sang-Eon, P.; Young-Sam, O., Methane reforming over Ni/Ce-ZrO<sub>2</sub> catalysts: effect of nickel content, *Applied Catalysis A: General*, **2002**, 226, 63-72.
- [16] Schulz, P.G.; Gonzalez, M.G.; Quincoces, C.E.; Gigola, C.E., Methane reforming with carbon dioxide. The behavior of Pd/ $\alpha$ -Al<sub>2</sub>O<sub>3</sub> and Pd-CeO<sub>x</sub>/ $\alpha$ -Al<sub>2</sub>O<sub>3</sub> catalysts, *Industrial and Engineering Chemistry Research*, **2005**, 44, 9020-9029.
- [17] Jong-San, C.; Do-Young, H.; Xinsheng, L.; Sang-Eon, P., Thermogravimetric analyses and catalytic behaviors of zirconia-supported nickel catalysts for carbon dioxide reforming of methane, *Catalysis Today*, **2006**, 115, 186-190.
- [18] Francisco, P.; Nora, N.N.; Mariana M.V.M.; Souza, D.V.C.; Osmar, A.F.; Martin, S., Study of Ni and Pt catalysts supported on  $\alpha$ -Al<sub>2</sub>O<sub>3</sub> and ZrO<sub>2</sub> applied in methane reforming with CO<sub>2</sub>, *Applied Catalysis A: General*, **2006**, 316, 175-183.
- [19] Jozwiak, W. K.; Nowosielska, M.; Rynkowski, J., Reforming of methane with carbon dioxide over supported bimetallic catalysts containing Ni and noble metal I. Characterization and activity of SiO<sub>2</sub> supported Ni-Rh catalysts, *Applied Catalysis A: General*, **2005**, 280, 233-244.

- [20] Sukkaew, C., Synthesis of nickel/magnesium/zirconium mixed oxide catalysts by co-precipitation method, Master Degree Dissertation, **2005**.
- [21] Mehran, R.; Seyed, M.A., Nanocrystalline zirconia as support for nickel catalyst in methane reforming with CO<sub>2</sub>, *Energy and fuel*, **2006**, 20, 923-929.
- [22] Mariana, M.V.M.S.; Donato, A.G.A.; Martin, S., Coke formation on Pt/ZrO<sub>2</sub>/Al<sub>2</sub>O<sub>3</sub> catalysts during CH<sub>4</sub> reforming with CO<sub>2</sub>, *Industrial and Engineering Chemistry Research*, **2002**, 41, 4681-4685.
- [23] Ding, R.G., Master Degree Dissertation, University of Petroleum, **1999**.
- [24] Shan, X.; Xiaolai, W., Highly active and coking resistant Ni/CeO<sub>2</sub>-ZrO<sub>2</sub> catalyst for partial oxidation of methane, *Fuel*, **2005**, 84, 563-567.
- [25] Rodriguez, J.A.; Wang, X.; Liu, G.; Hanson, J.C.; Hrbek, J.; Peden, C.H.F., Iglesias-Juez, A.; Fernandez-Garcia, M., Physical and chemical properties of Ce<sub>1-x</sub>Zr<sub>x</sub>O<sub>2</sub> nanoparticles and Ce<sub>1-x</sub>Zr<sub>x</sub>O<sub>2</sub> (111) surfaces: synchrotron-based studies, *Journal of Molecular Catalysis A: Chemical*, **2005**, 228, 11-19.
- [26] Laosiripojana, N.; Assabumrungrat, S., Methane steam reforming over Ni/Ce-ZrO<sub>2</sub> catalyst: Influences of Ce-ZrO<sub>2</sub> support on reactivity, resistance toward carbon formation, and intrinsic reaction kinetics, *Applied Catalysis A: General*, **2005**, 290, 200-211.
- [27] Rossignol, S.; Madier, Y.; Duprez, D., Preparation of zirconia-ceria materials by soft chemistry, *Catalysis Today*, **1999**, 2(29), 261-270.
- [28] Hyun-Seog, R.; Potdar, H. S.; Ki-Won, J.; Jae-Woo, K.; Young-Sam, O., Carbon dioxide reforming of methane over Ni incorporated into Ce-ZrO<sub>2</sub> catalysts, *Applied Catalysis A: General*, **2004**, 276, 231-239.
- [29] Crisafulli, C.; Scire, S.; Maggiore, R.; Minico, S.; Galvagno, S.; *Catalysis Letter*, **1999**, 59, 21.
- [30] Ashcroft, A.T.; Cheetham, A.K.; Green, M.L.H.; Vernon, P.D.F, Partial oxidation of methane to synthesis gas using carbon dioxide, *Letters to Nature*, **1991**, 352, 225-226.
- [31] Jin, H. J.; Jung, W. L.; Dong, J. S.; Yutaek, S.; Wang, L. Y.; Deuk, K. L.; Dong, H. K., Ru-doped Ni catalysts effective for the steam reforming of methane without the pre-reduction treatment with H<sub>2</sub>, *Applied Catalysis A: General*, **2006**, 302, 151-156.

- [32] Rostrup-Nielsen, J.R.; Sehested, J.; Norskov, J.K., Hydrogen and synthesis gas by steam-and CO<sub>2</sub> reforming, *Advances in Catalysis*, **2002**, 47, 65-139.
- [33] Rostrup-Nielsen, J.R.; Hansen, J.H.B., CO<sub>2</sub> reforming of methane over transition metals, *Journal of Catalysis*, **1993**, 144, 38.

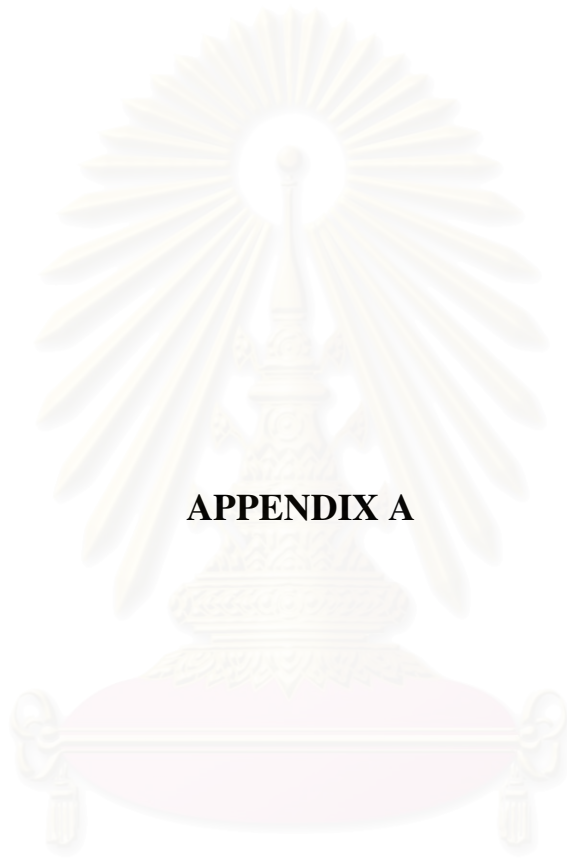


สถาบันวิทยบริการ  
จุฬาลงกรณ์มหาวิทยาลัย



**APPENDICES**

สถาบันวิทยบริการ  
จุฬาลงกรณ์มหาวิทยาลัย



**APPENDIX A**

สถาบันวิทยบริการ  
จุฬาลงกรณ์มหาวิทยาลัย

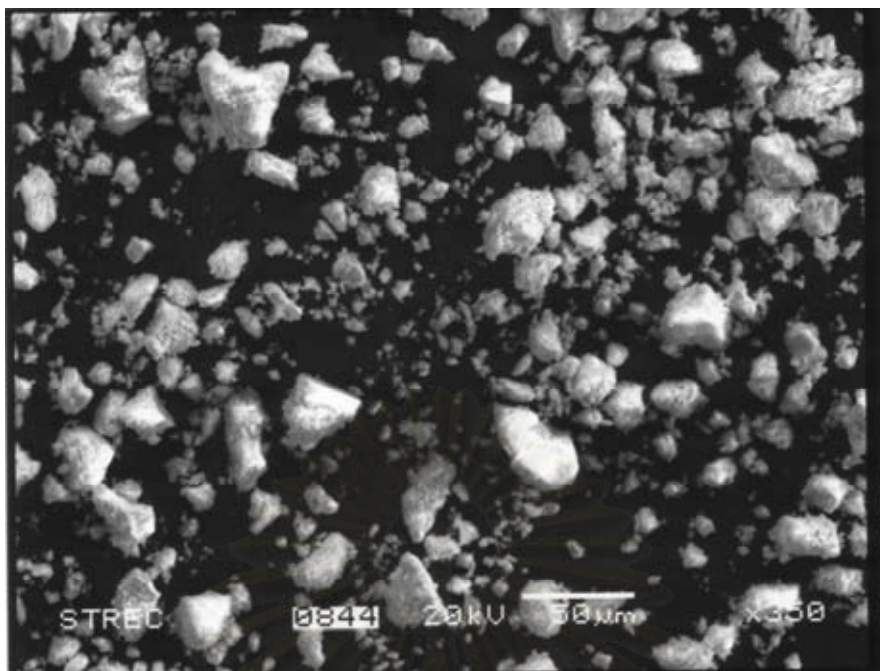


**Figure A-1** SEM of 0.3%Ru-15%Ni/Ce<sub>0.75</sub>Zr<sub>0.25</sub>O<sub>2</sub> catalyst.

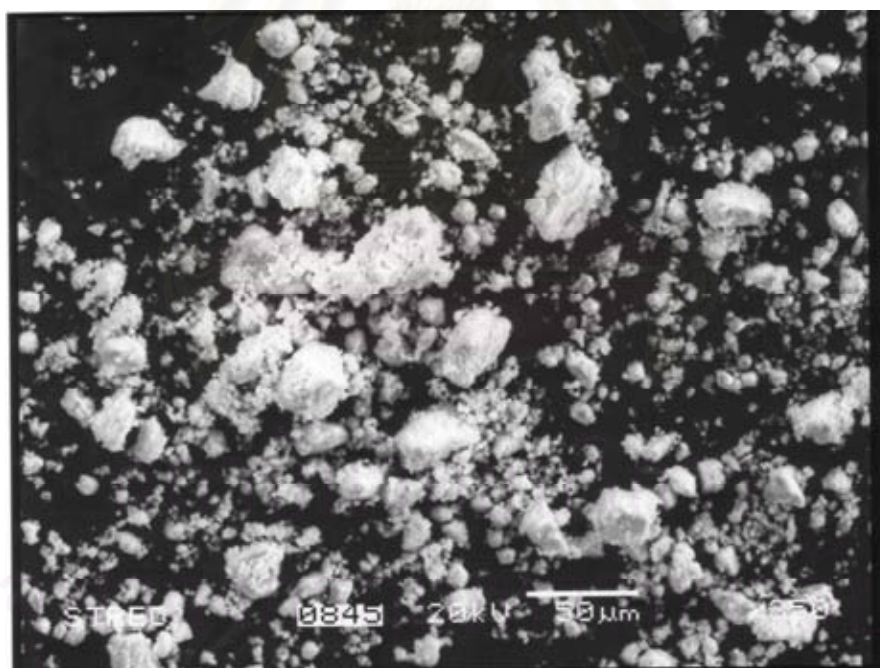


**Figure A-2** SEM of 0.5%Ru-15%Ni/Ce<sub>0.75</sub>Zr<sub>0.25</sub>O<sub>2</sub> catalyst.



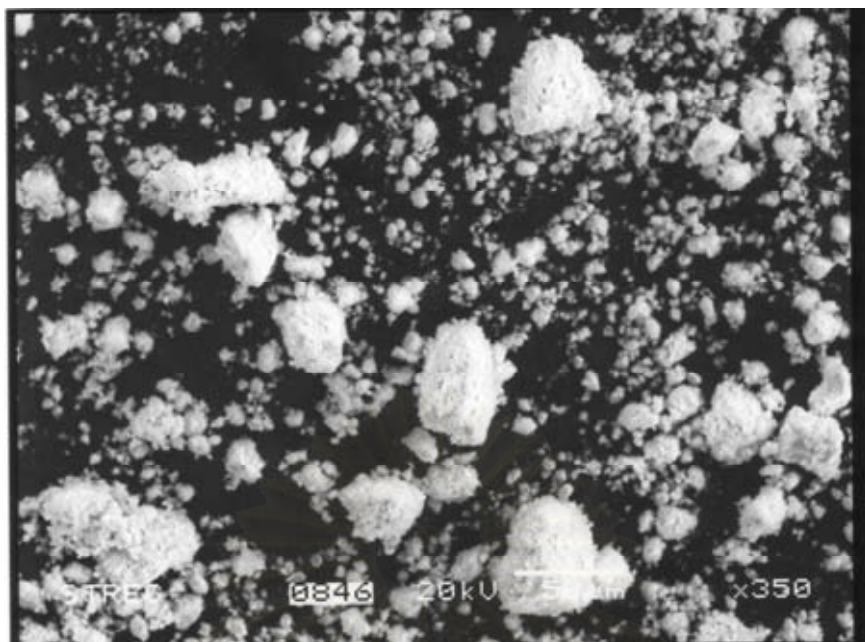


**Figure A-3** SEM of 0.7% Ru-15%Ni/Ce<sub>0.75</sub>Zr<sub>0.25</sub>O<sub>2</sub> catalyst.

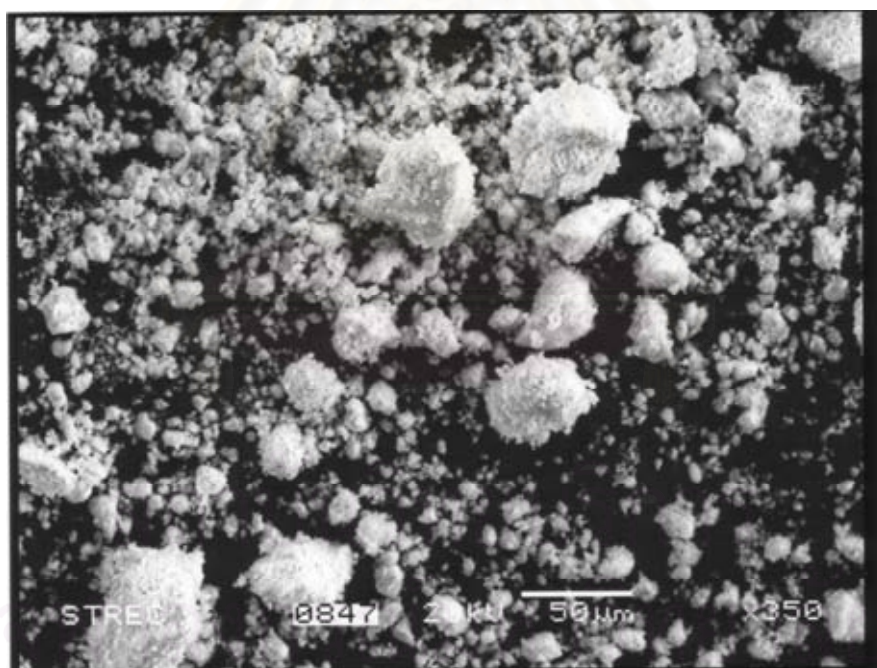
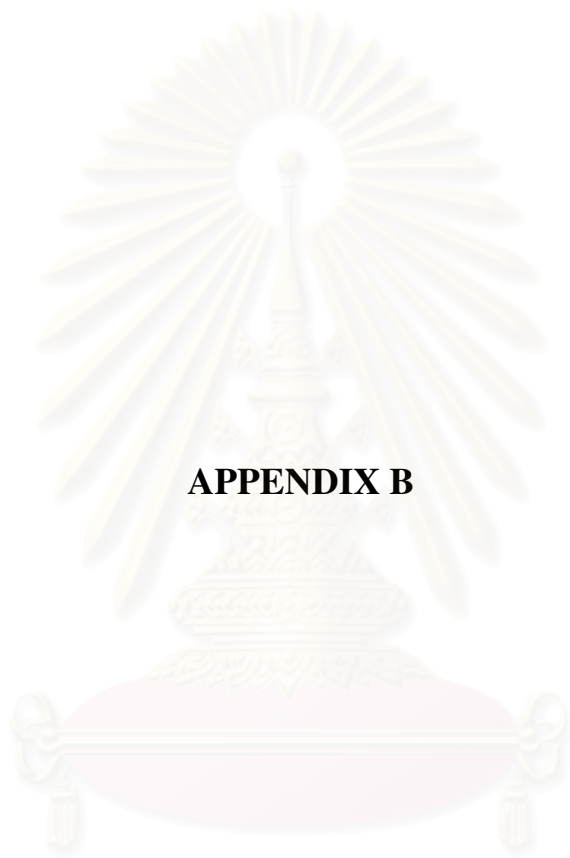


**Figure A-4** SEM of 1.0% Ru-15%Ni/Ce<sub>0.75</sub>Zr<sub>0.25</sub>O<sub>2</sub> catalyst.



**APPENDIX B**

สถาบันวิทยบริการ  
จุฬาลงกรณ์มหาวิทยาลัย

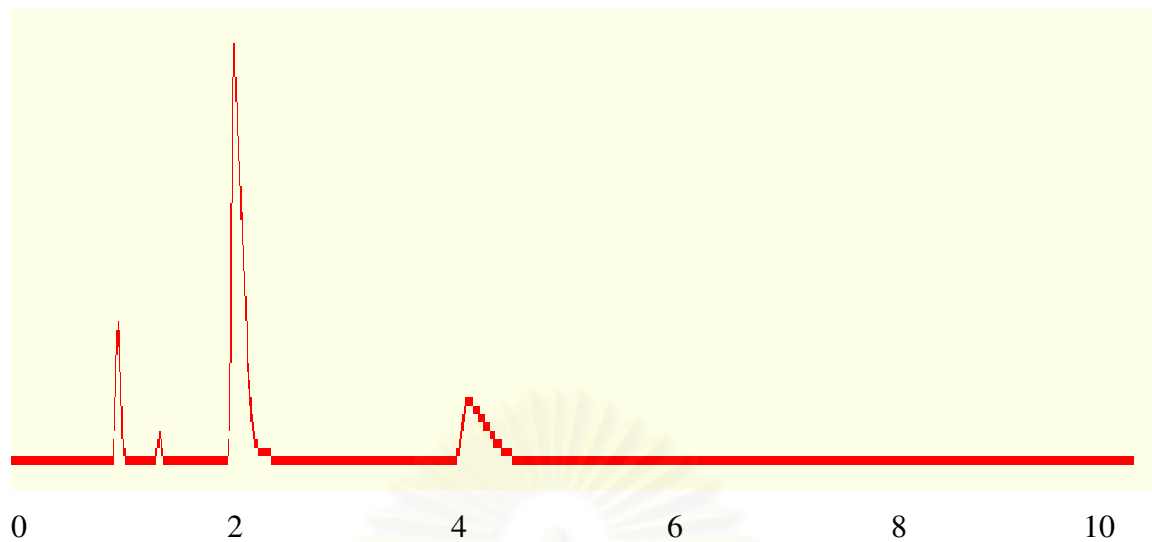


**Figure B-1** GC chromatogram over 15%Ni-0.3%Ru/Ce<sub>0.75</sub>Zr<sub>0.25</sub>O<sub>2</sub> catalyst after dry reforming of methane at 700 min, 450°C.

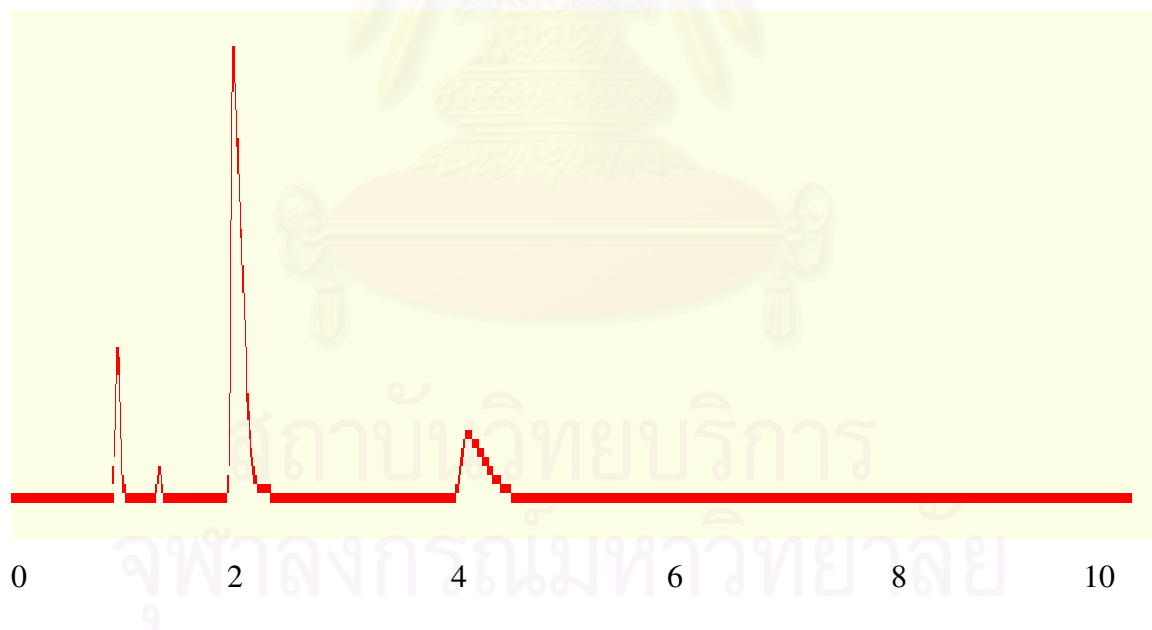


**Figure B-2** GC chromatogram over 15%Ni-0.5%Ru/Ce<sub>0.75</sub>Zr<sub>0.25</sub>O<sub>2</sub> catalyst after dry reforming of methane at 700 min, 450°C.

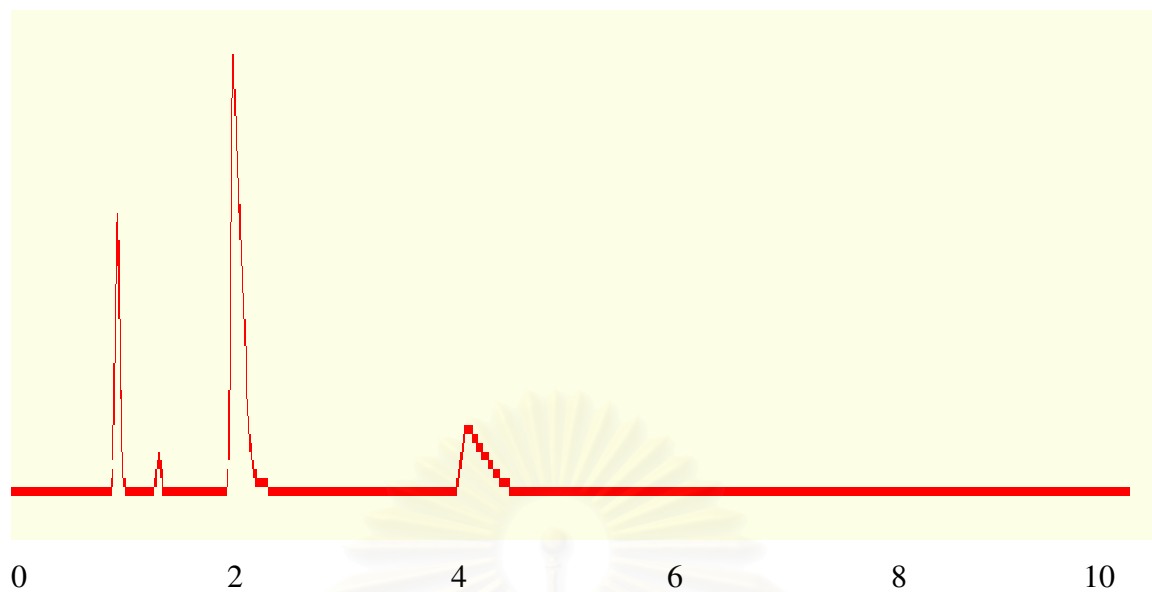


**Figure B-3** GC chromatogram over 15%Ni-0.7%Ru/Ce<sub>0.75</sub>Zr<sub>0.25</sub>O<sub>2</sub> catalyst after dry reforming of methane at 700 min, 450°C.

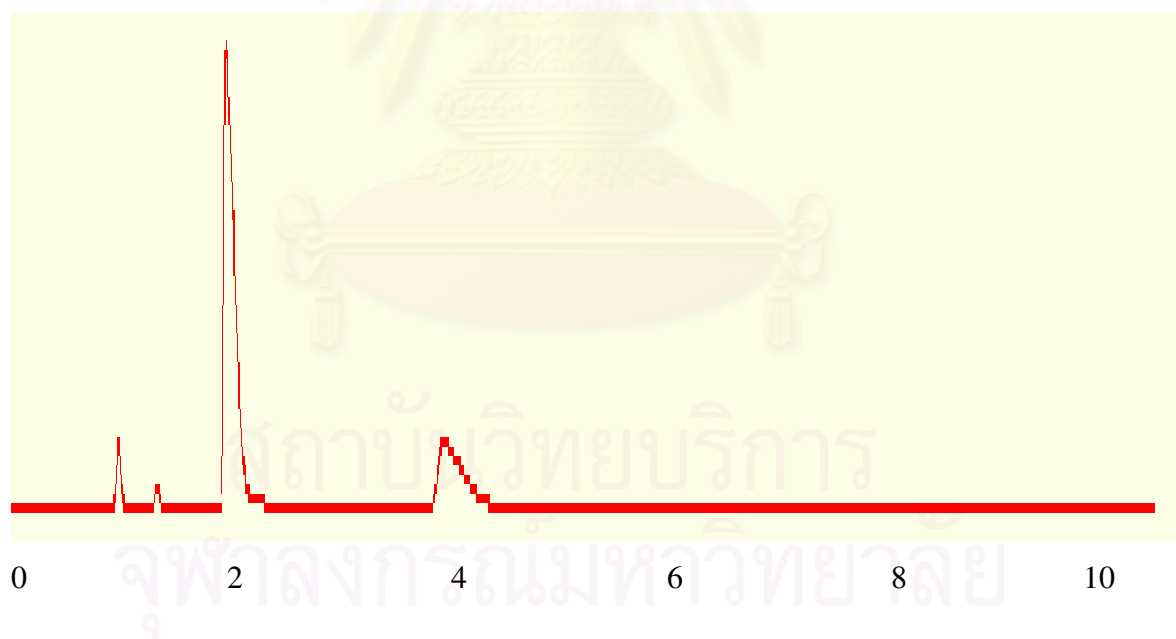
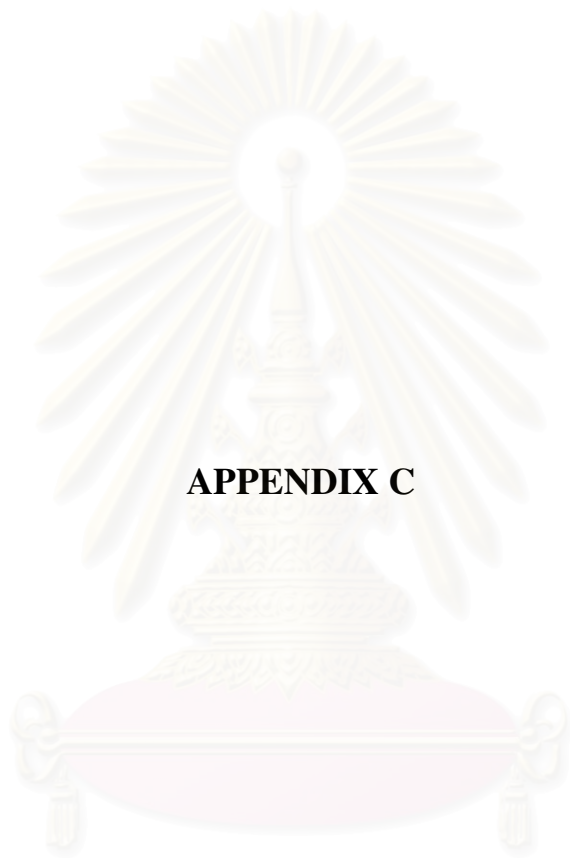


**Figure B-4** GC chromatogram over 15%Ni-1.0%Ru/Ce<sub>0.75</sub>Zr<sub>0.25</sub>O<sub>2</sub> catalyst after dry reforming of methane at 700 min, 450°C.



**APPENDIX C**

สถาบันวิทยบริการ  
จุฬาลงกรณ์มหาวิทยาลัย

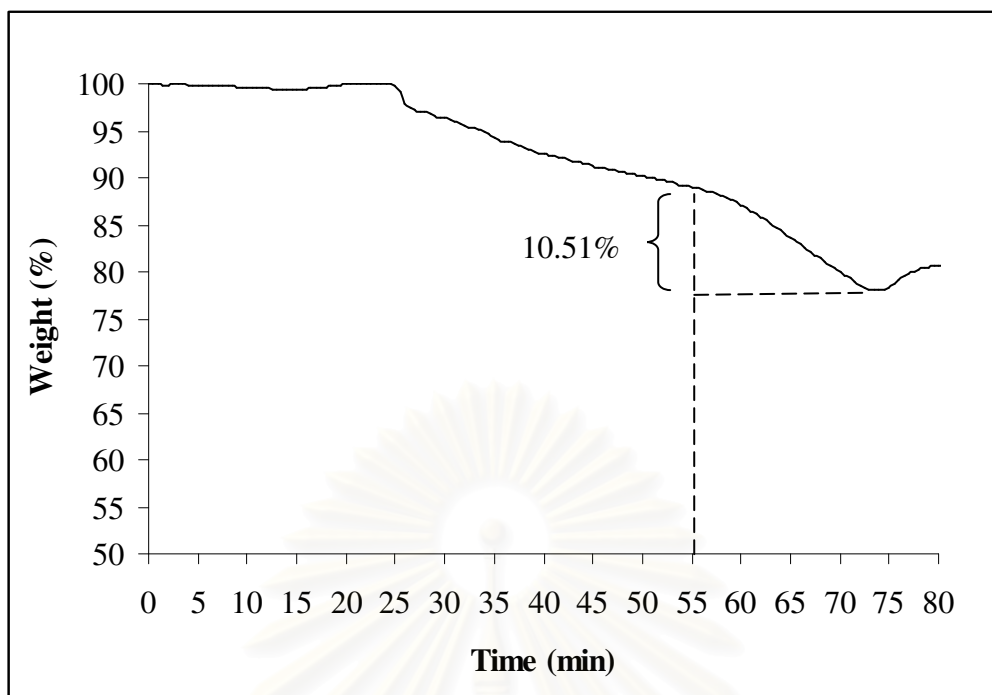


**Figure C-1** TGA profile over 15%Ni/Ce<sub>0.75</sub>Zr<sub>0.25</sub>O<sub>2</sub> catalyst after dry reforming of methane for 17 h at 450°C.

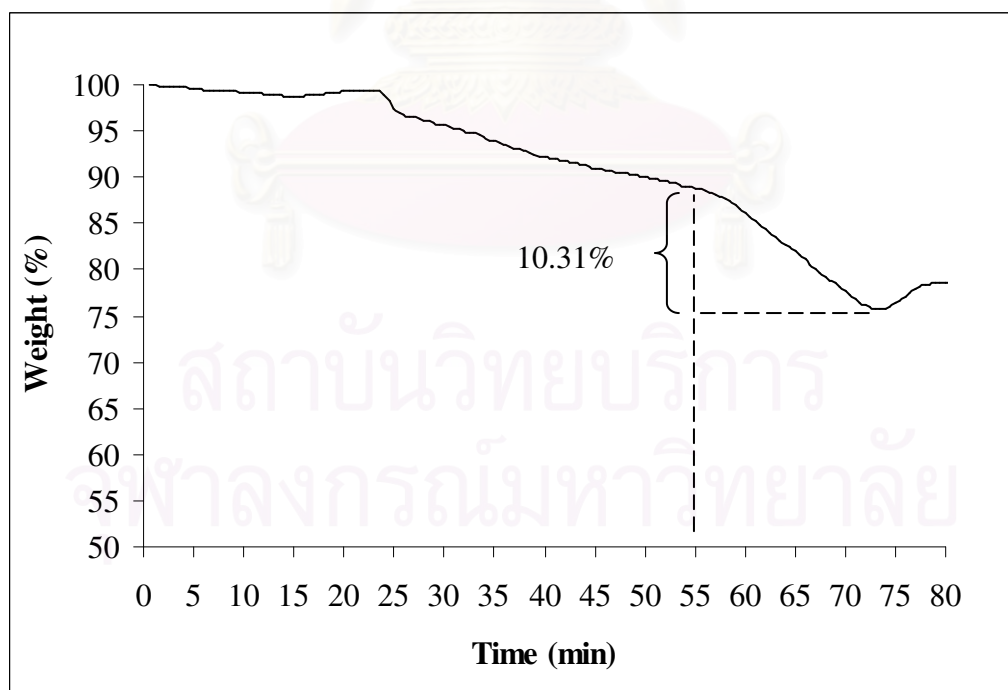


**Figure C-2** TGA profile over 15%Ni-0.3%Ru/Ce<sub>0.75</sub>Zr<sub>0.25</sub>O<sub>2</sub> catalyst after dry reforming of methane for 17 h at 450°C.

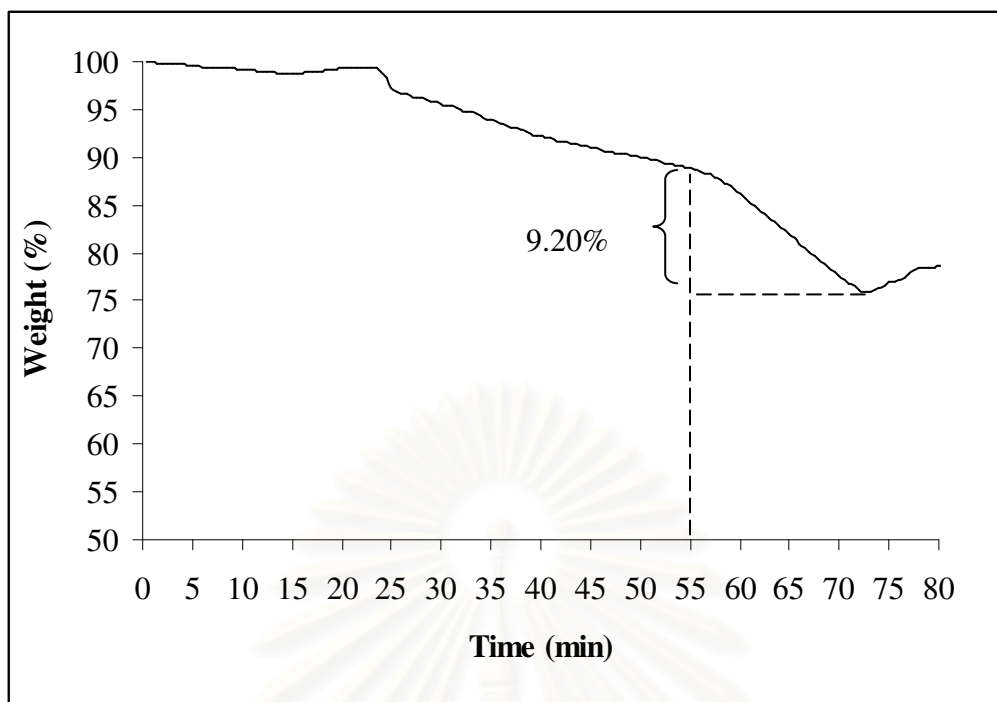


**Figure C-3** TGA profile over 15%Ni-0.5%Ru/Ce<sub>0.75</sub>Zr<sub>0.25</sub>O<sub>2</sub> catalyst after dry reforming of methane for 17 h at 450°C.

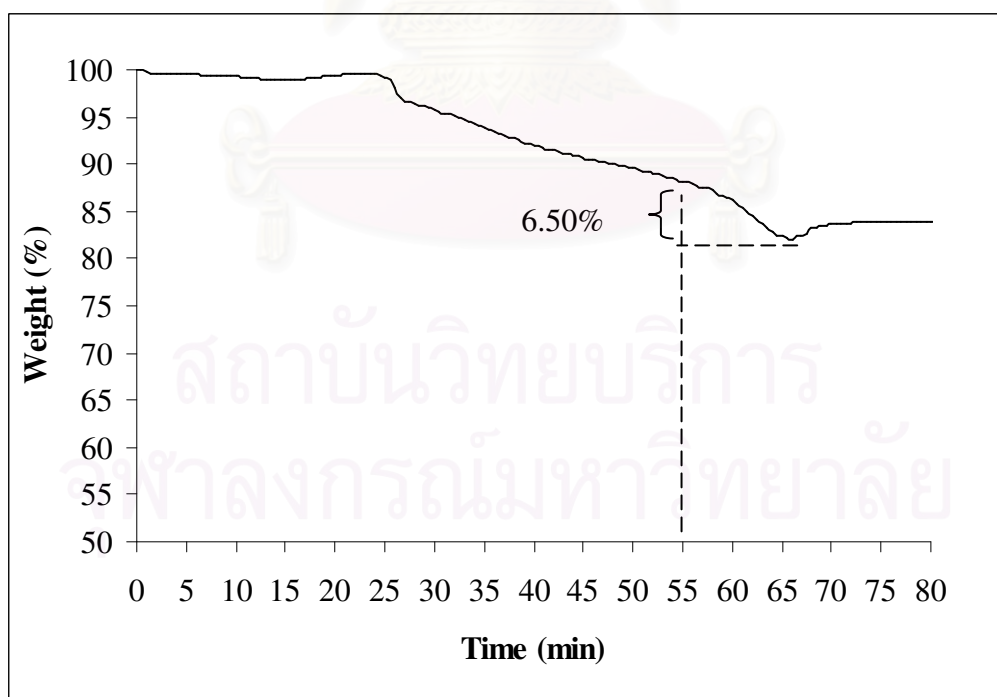


**Figure C-4** TGA profile over 15%Ni-0.7%Ru/Ce<sub>0.75</sub>Zr<sub>0.25</sub>O<sub>2</sub> catalyst after dry reforming of methane for 17 h at 450°C.

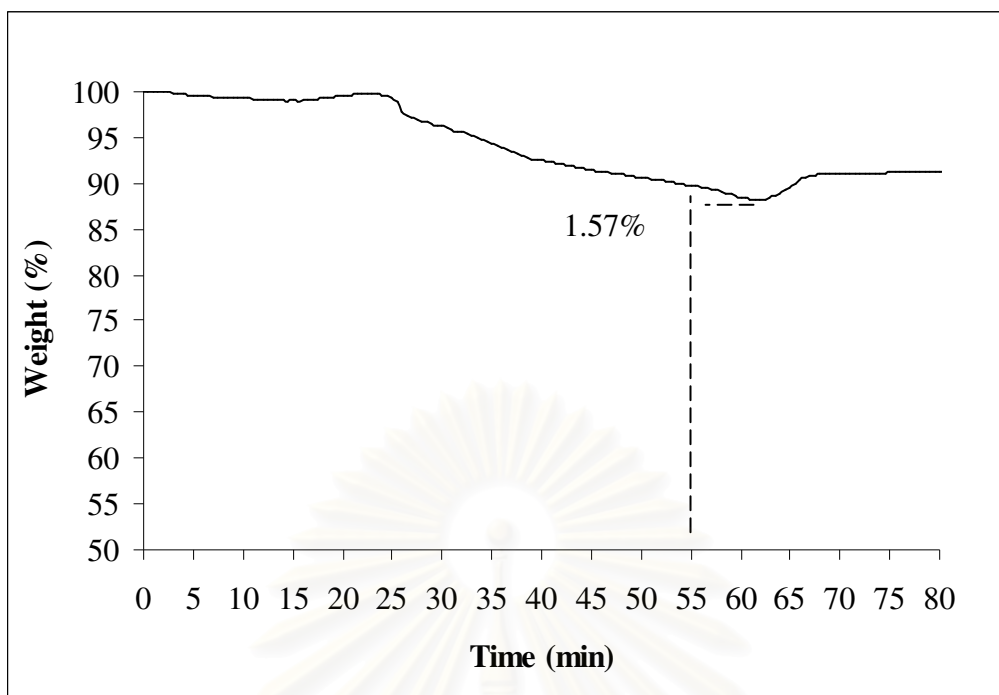


**Figure C-5** TGA profile over 15%Ni-1.0%Ru/Ce<sub>0.75</sub>Zr<sub>0.25</sub>O<sub>2</sub> catalyst after dry reforming of methane for 17 h at 450°C.

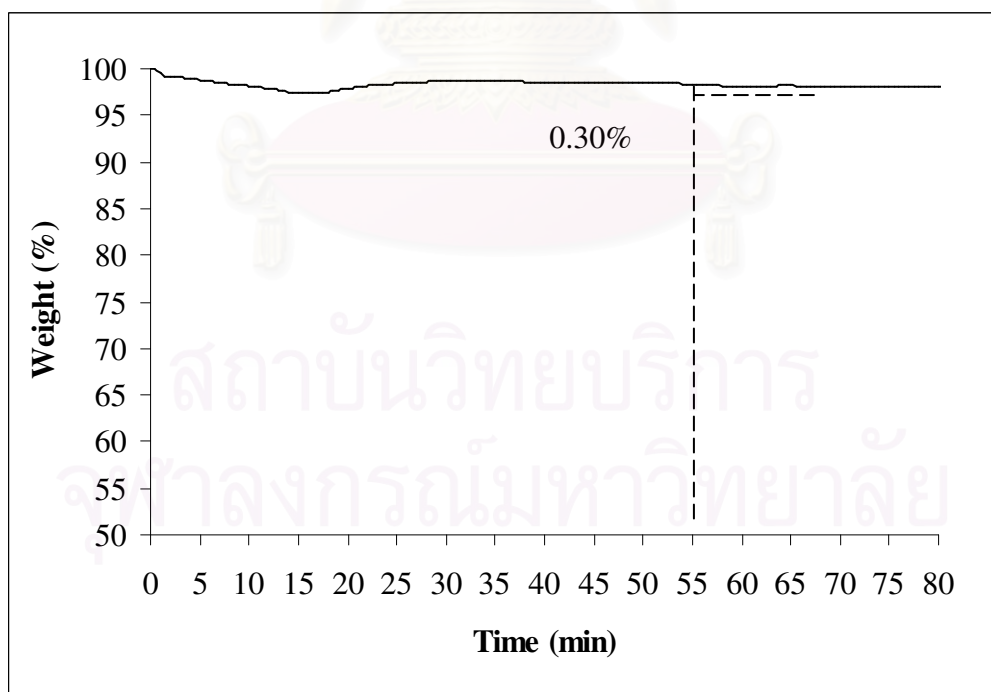


**Figure C-6** TGA profile over 1%Ru/Ce<sub>0.75</sub>Zr<sub>0.25</sub>O<sub>2</sub> catalyst after dry reforming of methane for 17 h at 450°C.



## VITA

Miss Yada Makhum was born in Bangkok, Thailand. She received the B.Sc. Degree in Chemistry Science at Mahidol University in 2004. Since then, she has been a graduate student studying in the program of Petrochemistry and Polymer Science at Faculty of Science, Chulalongkorn University. She completes her MS in 2007.



สถาบันวิทยบริการ  
จุฬาลงกรณ์มหาวิทยาลัย